

How Deep Can We See?

The Depth Penetrating Characteristics of Ground
Penetrating Radar

A Case History from Egypt's Mersa/Wadi Gawasis

By:

Glen Dash, Dash Foundation for Archaeological Research
Research Advisor to the Center for Remote Sensing, Boston University

Revision of September 30, 2008

Contents

LIST OF FIGURES	3
LIST OF TABLES	4
ADDENDA AND ERRATA	5
ACKNOWLEDGEMENTS	6
I: INTRODUCTION	7
II: GROUND PENETRATING RADAR BASICS	8
III: MERSA/WADI GAWASIS	12
IV: PREDICTING ABSORPTION LOSSES THROUGH NUMERICAL ANALYSIS	18
V: PREDICTING SCATTERING LOSSES WITH PSPICE	21
VI: PREDICTING LOSSES WITH ELECTROMAGNETIC WAVE SIMULATION	31
VII: THE 2006/2007 FIELD SEASON AT MERSA/WADI GAWASIS	36
VIII: CONCLUSIONS	44
APPENDIX A: A PRIMER ON THE PROPAGATION OF ELECTROMAGNETIC SIGNALS THROUGH SOILS	45
APPENDIX B: LOSS IN TRANSLATION	53
APPENDIX C: GPRMAX2D INPUT FILE	61
APPENDIX D: FLOWCHART FOR PROCESSING DATA IN GPR SLICE	62
REFERENCES	63

List of Figures

FIGURE 1: BLOCK DIAGRAM OF A GROUND PENETRATING RADAR SYSTEM.	9
FIGURE 2: LOSSES ANALYZED	10
FIGURE 3: QUEEN HATSHEPSUT	13
FIGURE 4: THE CAVES AT MERSA/WADI GAWASIS	14
FIGURE 5: THE SURROUNDING AREAS	15
FIGURE 6: PROFILE OF THE WESTERN SLOPE	17
FIGURE 7: A SIMPLIFIED MODEL OF THE STRATA	19
FIGURE 8: VELOCITY CHANGES CAUSE REFLECTIONS	22
FIGURE 9: A MORE COMPLETE MODEL OF LOSSES INCLUDING REFLECTION	24
FIGURE 10: USING PSPICE TO PREDICT SCATTERING LOSSES	26
FIGURE 11: A PROPAGATING ELECTROMAGNETIC WAVE	27
FIGURE 12: THE RESULTS OF THE PSPICE SIMULATION	29
FIGURE 13: A MODEL FOR USE IN GPRMAX2D	33
FIGURE 14: THE OUTPUT OF GPRMAX2D	34
FIGURE 15: RESULTS WITH AND WITHOUT CAVE PRESENT	35
FIGURE 16: 2006-2007 FIELD SEASON RESULTS	38
FIGURE 17: A SUBSURFACE RADAR PROFILE	39
FIGURE 18: WIGGLE TRACES AND RADARGRAMS	40
FIGURE 19: COMBINING INFORMATION FROM PARALLEL TRANSECTS	41
FIGURE 20: REFLECTED ENERGY PROFILE	42
FIGURE 21: MAP OF REFLECTED ENERGY FOR THREE PAIRS OF TRANSECTS	43
FIGURE 22: MAXIMUM DEPTH OF OBSERVATION FOR SEVERAL SOIL TYPES	49
FIGURE 23: CONDUCTIVITY AND PERMITTIVITY MEASURED	55
FIGURE 24: CONDUCTION AND DIELECTRIC CURRENTS	58
FIGURE 25: CONDUCTIVITY, PERMITTIVITY AND PHASE	60

List of Tables

TABLE 1: CALCULATION OF ABSORPTION LOSSES	20
TABLE 2: CALCULATING THE DEPTH OF OBSERVATION IN VARIOUS SOILS	48

Addenda and Errata

Readers can find addenda and errata at:

<http://www.DashFoundation.org/HowDeep/Errata.html>.

Acknowledgements

I am grateful to Professor Kathryn Bard of the Department of Archaeology at Boston University and Professor Rodolfo Fattovich of the University of Naples “L’Orientale” (UNO) for inspiring this project, providing access to the site, helping with logistics and reviewing this report.

This work would not have been possible without the efforts of geophysicist and archaeologist Benjamin Vining (Boston University) who joined me during the 2005-2006 season at Mersa/Wadi Gawasis and who conducted the 2006-2007 survey.

I am also grateful to the archaeologists and specialists who assisted me in understanding the geological and archaeological aspects of the site, including Trina Aprin (Boston University), geoarchaeologist; S. Terry Childs (US National Park Service, Washington D.C.), archaeologist and archaeometallurgist; Andrea D’Andrea (UNO), surface surveyor; Rainer Gerisch (Free University, Berlin, Germany,) paleobotanist; Elsayed Mahfouz (University of Assyut, Assyut, Egypt), Egyptologist; Andre Manzo (UNO), archaeologist; Carla Pepe (University “Suor Orsola di Benincasa”, Naples, Italy), archaeologist; Cinzia Perlingieri (UNO), archaeologist, ceramic analyst and illustrator; Stefano Tilia (Terre, Rome, Italy), surface surveyor; and Cheryl Ward (Florida State University, Tallassee, USA), nautical archaeologist.

I am most grateful to Dr. Dean Goodman, the author of the GPR-Slice software, for his review of this publication and to Betsy Mattheissen for skillfully proofreading this report.

I would also like to thank Dr. Farouk El-Baz, Director of the Center for Remote Sensing at Boston University for offering me the opportunity to serve as Research Advisor to the Center and for his suggestion that karst formations at Mersa/Wadi Gawasis may be more easily detected than the caves themselves.

Finally, I would like to thank Dr. Joan Dash, soil scientist and photographer, and Rebecca Dash (Rensselaer Polytechnic Institute, Troy, NY, USA) for assisting with logistics and data collection.

I. Introduction

The Wadi Gawasis runs into the Red Sea just south of Safaga in Egypt. In 1977, A. M. Sayed identified this place as the location of the harbor (or Mersa) Gawasis from which the Egyptian Pharaohs of the Middle Kingdom launched their sea voyages to the east and south. In 2001, Professors Kathryn Bard of Boston University and Rodolfo Fattovich of University of Naples “L’Orientale” (UNO) began their excavations at Mersa/Wadi Gawasis, mapping portions of its 20-hectare extent. On December 25, 2004, Kathryn Bard punched through a layer of overburden on the western side of a coral terrace, discovering the first of seven known caves. Inside these, Drs. Bard and Fattovich have since found, among other things, cedar ship timbers and fiber ropes in a remarkable state of preservation, the latter all neatly bundled and stowed away.

In 2005, Dr. Bard asked me if remote sensing could be employed to find additional caves. If they were like the others, they would lie five to six meters below the surface of the terrace. Although we could employ electromagnetic induction, magnetometry and ground penetrating radar to the task, it was unclear whether any of these technologies would work. Given the current technology, five to six meters is still a long way down.

But in addition to these challenges, the site also offered some unique opportunities. The coral terrace at Mersa/Wadi Gawasis has well-defined, exposed strata. We knew that if we were able to measure the electrical properties of each individual stratum, we could predict which of the technologies would work best. During our 2005-2006 geophysical season, we measured their properties with electromagnetic induction tools. From this we were able to conclude that radar would be our best bet.

To determine just how well radar would work, we employed simple numerical models to predict absorption losses, PSPICE, a software tool borrowed from electrical engineers to predict scattering losses, and finally GprMax2D to predict the overall results.

In 2006-2007, we gathered our field data and analyzed it using GPR-Slice. We found that we could detect the caves despite their depth, due in part to the practical nature of their builders. They carved the caves out of rock that had been softened by water percolating down from the top of the terrace. Although the caves themselves would have been difficult to detect, the fingerprint of this water movement was plainly visible.

In the end, Mersa/Wadi Gawasis has become both an archaeological site and a kind of geophysical laboratory. Here, in close proximity to the profiles we wish to map are exposed sections of the subsurface. This combination gives us a rare opportunity to both predict results and test those predictions.

II: Ground Penetrating Radar Basics

Ground Penetrating Radar (GPR) is sometimes aptly referred to as “electromagnetic sounding.” GPR works much the way early underwater acoustic sounding (sonar) devices worked, although with radio waves rather than sound. Early sonar gear worked through a process known as “pinging.” A surface ship used an acoustic transmitter to produce a ping, and an acoustic receiver to listen for a return. The distance to the target could be calculated if the speed of sound in water was known,

Most ground penetrating radar devices used in archaeological surveys work in an analogous way. They have a transmitter that produces an electromagnetic ping that travels down through the soil, and a receiver which listens for a return. If the velocity of the electromagnetic ping is known, the distance to the target can be calculated.

Both types of devices – acoustic and electromagnetic -- have the same basic benefits and drawbacks. They are simple to build and operate, and can be quite accurate provided the velocity of the ping is known. Unfortunately, that velocity can sometimes be difficult to estimate, especially in the case of electromagnetic waves. Furthermore, neither technique is especially deft at determining the angle to the target. Generally, they use a transmitter with a broad “beam width” which illuminates a wide area without discrimination, more like a flashlight than a laser beam.

In a typical GPR system, the ping produced by the transmitter is a pulse of radio frequency energy known as a “wavelet.” This is used to energize a transmitting antenna (Figure 1). The returning signal is picked up by the receiving antenna and is coupled to a radio frequency receiver. A signal processor helps separate the signal from the noise, and the user views the results on a display.

How deep can we expect to see? That depends on how much signal is lost along the way. According to David Daniels, a sensors specialist, there are seven types of signal loss we need to consider (Daniels 2004:15, Figure 2).

The first of these are “antenna losses.” Not all the power produced by the transmitter is converted into radiated energy by the transmitting antenna; some is dissipated in the form of heat. Daniels states that 30 percent of the energy is lost this way. By convention, this loss is expressed as decibels (dB):

$$Loss(dB) = -20 \log(S_{out} / S_{in})$$

$$S_{out} / S_{in} = .7$$

$$Loss(dB) = 20 \log(.7) = 3dB$$

Where:

$Loss(dB)$ = Loss in decibels

S_{out} = Signal radiated from the antenna

S_{in} = Signal fed into the antenna

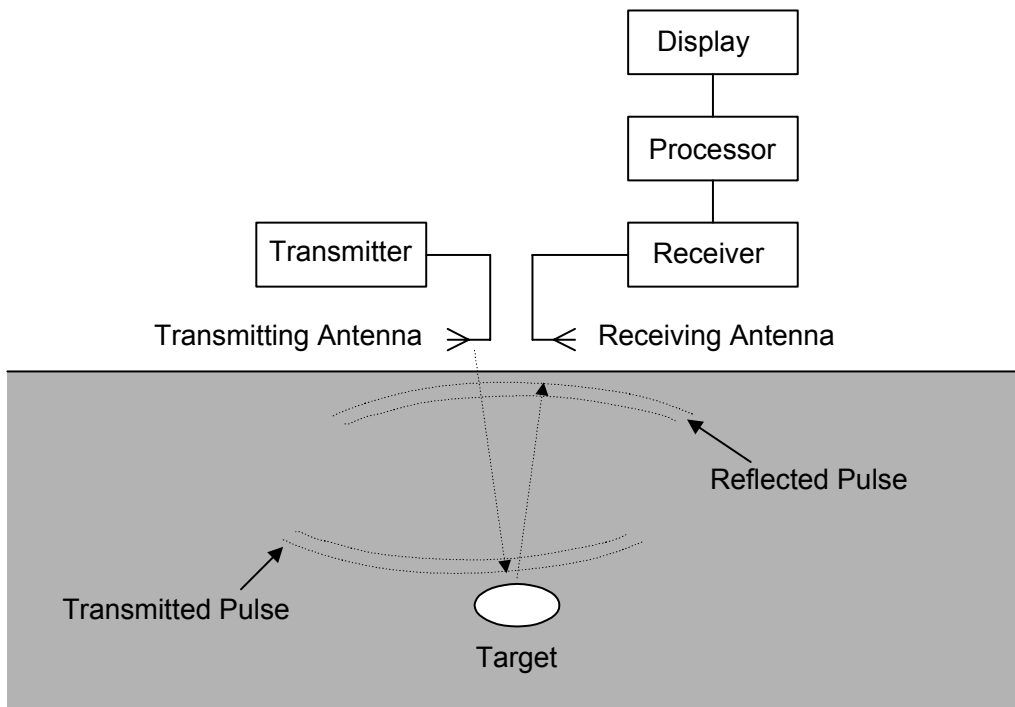


Figure 1: Block diagram of a Ground Penetrating Radar system.

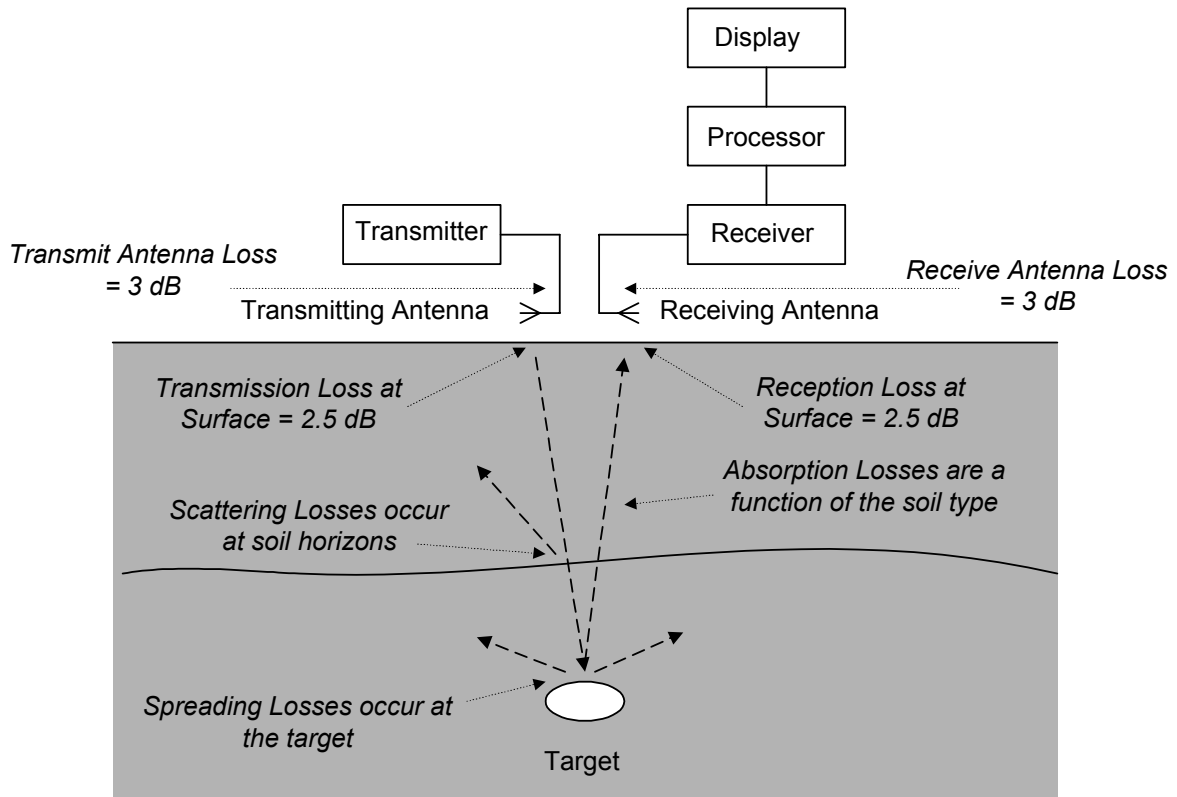


Figure 2: Losses which must be considered in predicting whether Ground Penetrating Radar will work in a given application.

A similar phenomenon occurs on the receiving end, so the antenna losses total 6dB.

Secondly, not all the signal radiated from the antenna actually penetrates into the ground. Some of it reflects off the ground surface into the air. Daniels estimates this “transmission loss” at 2.5dB typically. Since the reverse happens on the receiving side, we lose an additional 5dB.

As the signal travels downward toward the target, it may encounter distinct soil layers. Some of the signal will be reflected off the interface between these layers and will never return. This is known as “scattering loss.”

Part of the energy that does reach the target will be reflected back towards the receiving antenna, but part will be reflected away, absorbed by the target or will pass through it. These are known as “spreading losses.”

Finally, a good portion of the signal is just dissipated away by the passage through the soil itself. These are “attenuation losses.”

All together, our losses are:

$$L_T = L_{ant} + L_t + L_{sc} + L_s + L_a$$

Where:

L_T = Total loss in dB

L_{ant} = Antenna losses in dB (typically 6dB)

L_t = Transmission losses in dB (typically 5dB)

L_{sc} = Scattering losses in dB

L_s = Spreading loss in dB

L_a = Attenuation losses in dB

Most GPR systems can tolerate 60 to 80dB of total loss; any more than that and the returning signals will be lost in the noise. Because our antenna and transmission losses will cost us about ~10dB, a target *may* be detectable under optimum conditions if the remaining losses total less than ~70dB and *should* be detectable under most conditions if the remaining losses total less than ~50dB. Whether or not the total loss will be less than these values depends on the attenuation, spreading and scattering losses particular to a given site.

III: Mersa/Wadi Gawasis

Hatshepsut, Egypt's great Pharaoh Queen (ca. 1473-1458 BC), built her mortuary temple at Deir el-Bahri, just outside the Valley of the Kings. The walls of her temple are decorated with striking depictions of an expedition undertaken during her reign to the fabled land of Punt.

Punt was an exotic land to the south; even today no one knows exactly where it was located. The Egyptians described it as a land where the people lived in beehive-shaped reed huts. From here came marvelous things: frankincense, myrrh, electrum, gold and ebony, in vast quantities. "Millions, hundred-thousands, ten thousands, thousands and hundreds [are the] marvels of Punt" (Bard and Fattovich 2007:19).¹ Some expeditions brought back the skins of giraffes, panthers and cheetahs, some to be worn by temple priests. Other expeditions brought back the animals themselves. Occasionally, humans were included in the cargo.

These sea voyages were a recurrent theme in Egyptian texts with references going back to reign of Pepi II (ca. 2278-2184). During Egypt's Middle Kingdom (ca. 2040-1640 BCE) Egypt's Pharaohs launched numerous expeditions, some reportedly involving as many as 3,000 men (Bard and Fattovich 2007:20).²

In 1976 and 1977, Abdel Moneim Al-Hakim Sayed of the University of Alexandria explored the mouth of the Wadi Gawasis, 23 kilometers south of the town of Safaga on the Red Sea (26°33'26"N, 34°02'11"E). This place had previously been identified as the Roman port of Philoteris (Bard and Fattovich 2007:23 citing Tregenza 1958: 182). Here Sayed found inscribed potsherds, wood, limestone anchors and stelae in sufficient quantity to determine that this place was a seafaring port during Egypt's 12th Dynasty (Bard and Fattovich 2007:23).³

Since 2001, Professor Kathryn Bard of Boston University and Professor Rodolfo Fattovich of the University of Naples "L'Orientale (UNO)) have completed several seasons of field investigations at Mersa/Wadi Gawasis. They have identified an ancient site spread over 20 hectares, crisscrossed by a modern road and railway which divide it into eastern, central and western sectors. Much of their work has focused on a rock terrace, where they found ceramics and lithics in great abundance.

In 2004, Dr. Bard happened upon the first of Mersa/Wadi Gawasis' caves hidden beneath two meters of overburden. As of 2008, seven caves have been identified, each carved into bedrock along the western slope of the terrace.

¹ Bard and Fattovich cite Naville 1898 and Breasted 1906-7.

² Bard and Fattovich cite Bradbury 1988, Sayed 2003, Jones 1995, Vinson 1994 and Ward 2000.

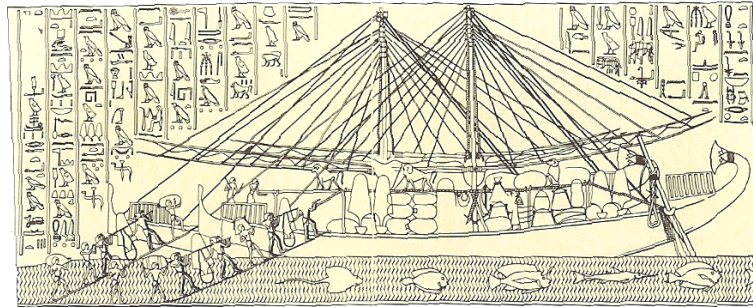
³ Bard and Fattovich cite Sayed 1977, 1978, 1979a, 1979b, 1980, 1983 and 1999.



(a)



(b)



(c)



(d)



(e)

Figure 3: Clockwise from the upper left: Queen Hatshepsut, shown making an offering to the gods, built her mortuary temple into the cliffs at Deir el-Bahri outside the Valley of the Kings. Her ships carried back great quantities of the “marvelous things from Punt” from incense to wild animals. She had the figure of the obese Queen of Punt recorded on her Temple’s walls. (Credits: (a), (b) Parsons M. “Deir el-Bahri,” <http://www.touregypt.net/featurestories/bahri.htm>; (c) Clayton 1994; (d), (e) Dunn, J. “The Wonderful Land of Punt,” <http://www.touregypt.net/featurestories/punt.htm>)

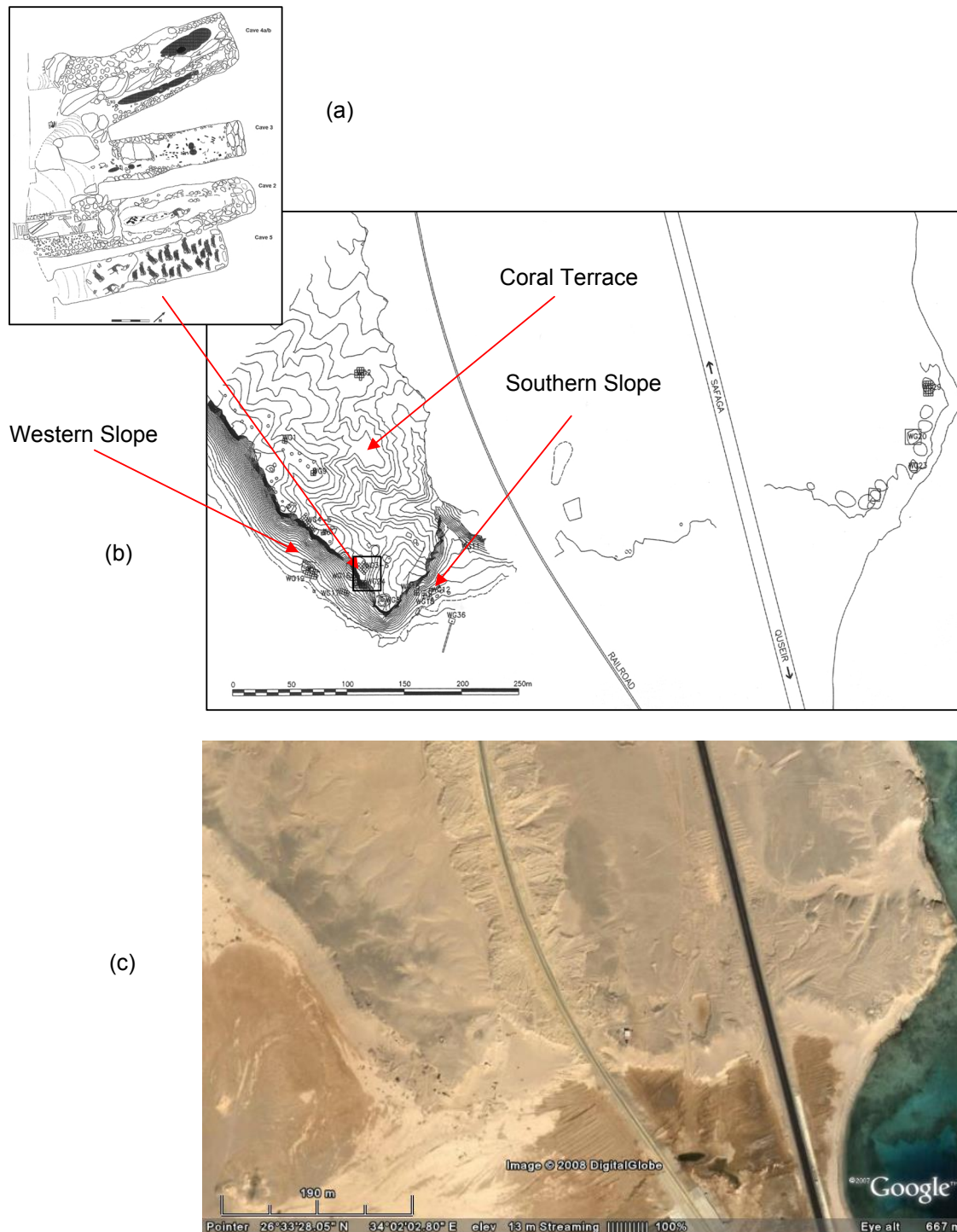


Figure 4: Archaeologists found caves at Mersa/Wadi Gawasis embedded in the western slope (actually the south-western slope) of a coral terrace. (Credits: (a), (b) Bard and Fattovich 2007, (c) Google 2008)



(a)

Wooden
Rudder



(b)



(c)



(d)

Figure 5: The caves and the surrounding areas at Mersa/Wadi Gawasis have yielded remarkably preserved ropes, ship timbers, stone anchors and even shipping boxes, one of which bore the inscription “Wonderful Things from Punt.” (Credits: (a), (b), (d) Bard and Fattovich 2007, (c) photo by the Dash Foundation, 2006)

The caves contained extraordinary artifacts. In Cave 2, excavators discovered ship timbers presumably from the very ships which had gone to Punt. Some of the timbers show evidence of rework, presumably to make them ready for the next sea voyage (Bard and Fattovich 2007: 62-66). In Cave 5, archaeologists C. Perlingieri and C. Zazzaro discovered dozens of coils of remarkably preserved rope, each carefully bundled and stowed away to for the next sea journey.

The primary goal of our 2005-2006 and 2006-2007 geophysical seasons at Mersa/Wadi Gawasis was to develop a method for detecting additional caves. As a practical matter, the easiest way to do this was from the top of the terrace.

Figure 6 shows the western slope of the terrace at the time of the survey (Vining 2005-2006). Above the entrance to Cave 2 there are five layers of rock strata. The topmost layer, designated Stratum 1, is thin and consists of gravel, alluvium and lag deposits. Beneath that is a two meter plus layer of porous fossil coral (Stratum 2), supported by a layer of massive coral (Stratum 3). Stratum 4 consists of beach conglomerate. The cave is cut into Stratum 5, which consists of massive conglomerate.

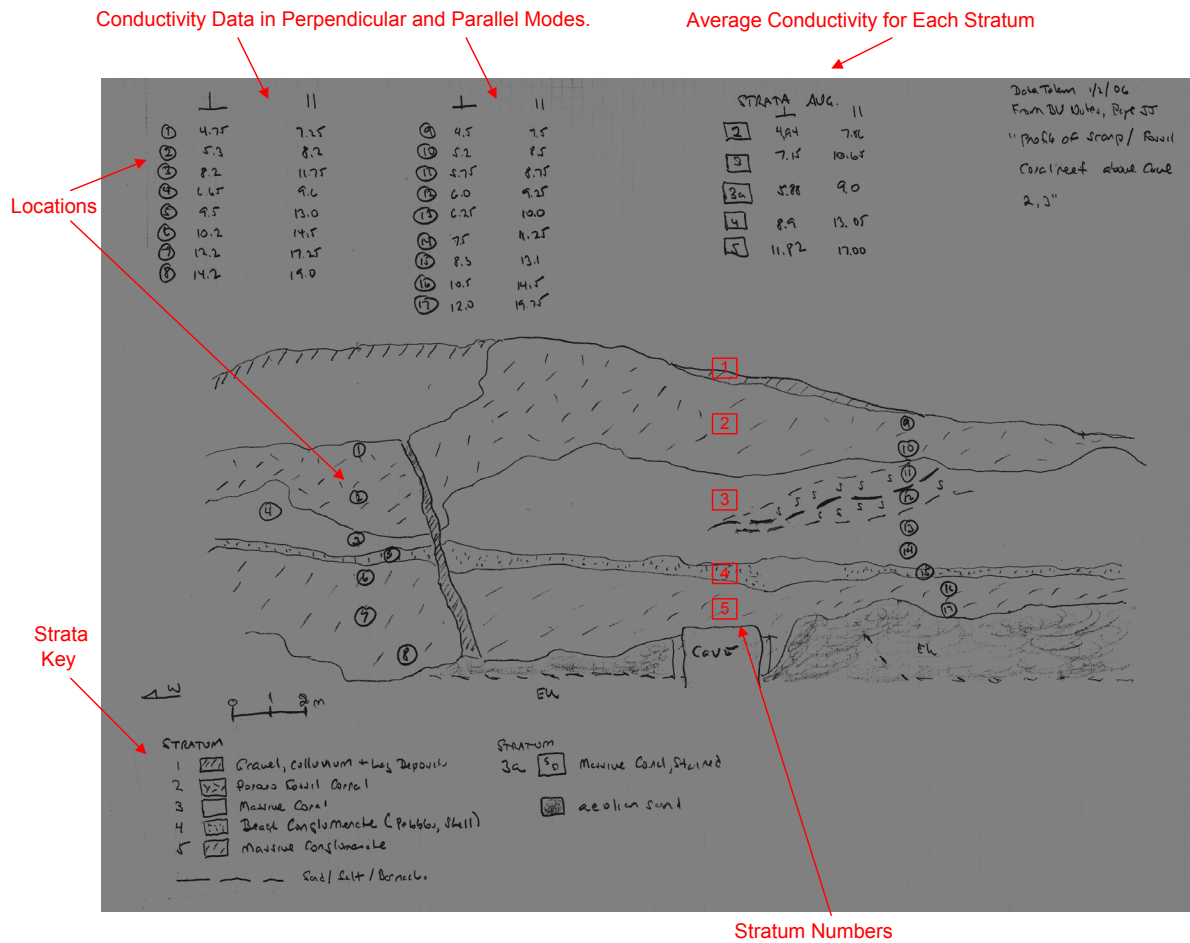


Figure 6: Profile of the western slope of the terrace at Mersa Gawasis showing the locations where conductivity data was collected. We measured the conductivity using a Geonics EM-31 probe in both perpendicular (\perp) mode and parallel (\parallel) mode. (Credit: Dash 2005-2006 as transcribed from Vining 2005-2006)

IV: Predicting Absorption Losses through Numerical Analysis

Whether or not we could successfully use radar to detect the caves at Mersa/Wadi Gawasis would depend on the nature of the soil we found there.

In electrical terms, we classify soils using three parameters: *conductivity*, *permittivity* and *permeability*.

Conductivity (σ) is a measure of how easily electrical current moves through a medium. As a general rule, the higher the soil's water content and salt concentration, the greater the conductivity. Soil conductivity is measured in Siemens per meter (or equivalently, mhos per meters).

Permeability (μ) is a measure of how easily a medium can be magnetized. Most soils have fairly low concentrations of iron and other ferrous metals and therefore cannot be easily magnetized. In fact, at the frequencies we will use, the magnetic properties of soil are about the same as air. Permeability is measured in units of Henries/meter and for air it is about equal to $4\pi \times 10^{-7}$ Henries/meter.

Permittivity (ϵ) is a measure of how easily a medium can be electrically charged. Permittivity is measured in units of Farads/meter and the permittivity of air is about the same as a vacuum, 8.85×10^{-12} Farads/meter. The permittivity of soils varies considerably and is strongly influenced by their water content. Materials are usually rated in terms of *Relative Permittivity* (κ), which is the permittivity relative to a vacuum. Soils generally vary in relative permittivity from 2 to 25.

During our 2005-2006 survey, we measured the conductivity of the strata using an EM31 electromagnetic induction meter. We placed the meter up against the vertical surface of the terrace at the points indicated in Figure 6. We took a total of 17 measurements, half of them in "parallel" (\parallel) mode and half in "perpendicular" (\perp) mode. The mode refers to the direction of the magnetic field produced by the instrument in relation to the plane of the surface. A perpendicular field penetrates farther into the soil but covers less area. A parallel field covers more area, but penetrates less deeply. For our purposes, we deemed the perpendicular measurements most relevant, since they penetrate farther into the terrace and have less of a tendency to cross layers.

Using this conductivity data, we were able to construct the simplified electrical model of the strata at Mersa/Wadi Gawasis shown in Figure 7.

We could only estimate the permittivity of the strata. Daniels states that the relative permittivity of dry, sandy soils varies from 4 to 10 (Daniels 2004: 90). We also know that both permittivity and conductivity rise with water content. Therefore, we assigned a relative permittivity of four to the uppermost layer in our model (Stratum 2), and ten to the bottom layer (Stratum 5). We used interpolation to estimate the permittivity of the intervening layers.

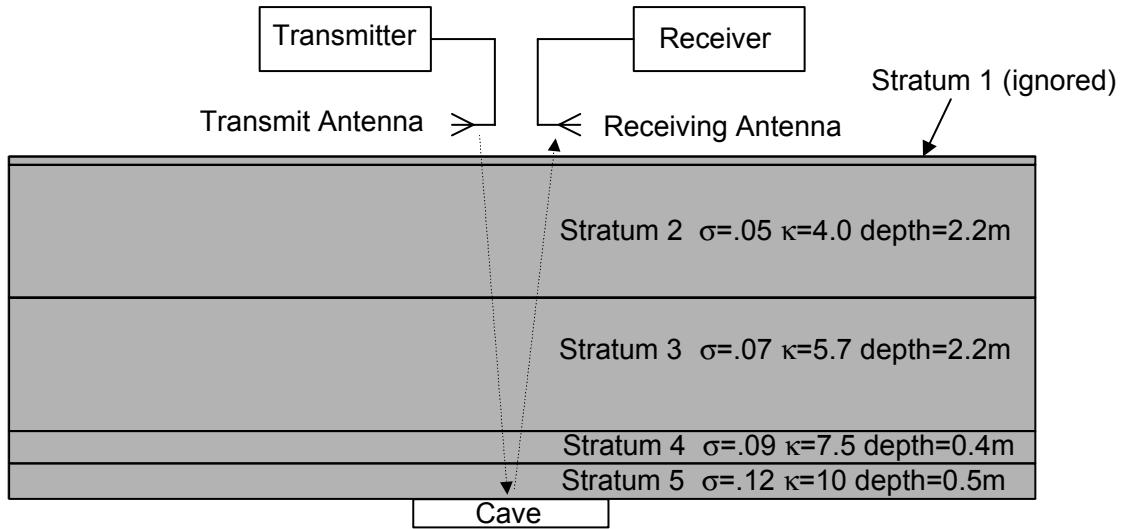


Figure 7: A simplified model of the strata at Mersa/Wadi Gawasis. The radar signal travels through a thin surface layer (which is ignored in the analysis) and four subsurface layers of varying properties. It reflects off the air-filled cave and returns to the surface.

From Appendix A we know that the absorption loss for each stratum is:

$$Loss(dB/m) = \frac{1.64\sigma_m}{\sqrt{\kappa}}$$

Where:

σ_m = Conductivity in milli-Seimens (1 σ = 1000 σ_m)

We used the values for relative permittivity and conductivity in Figure 7 to produce Table 1. As the signal passes through Stratum 2, all but 35.5 percent is lost, or in terms of decibels 9.0 dB. An additional 10.6 dB is lost in Stratum 3 and 2.16 dB in Stratum 4. By the time the signal reaches the cave, we have lost a total of 24.8 dB. (Since the losses are measured in terms of decibels and decibels are logarithmic, we can simply add them.) Even in the best case, where the entire signal that reaches the cave is reflected off it and back to the surface, we predict we will lose 49.7 dB to absorption.

Absorption Losses at Mersa/Wadi Gawasis*					
Stratum	Conductivity (mS)	Relative Permittivity	Depth (m)	Transmission (Linear)	Loss (dB)
2	5	4	2.2	0.355	-9.02
3	7	5.7	2.2	0.296	-10.58
4	9	7.5	0.4	0.781	-2.16
5	12	10	0.5	0.699	-3.11
Total					-24.87
Total (Round Trip)					-49.73
*Calculated assuming soil is of dielectric type					

Table 1: Calculation of Absorption Losses

However, this analysis merely accounts for absorption losses. Next we need to consider scattering losses and for that purpose we used a program known as PSPICE.

V: Predicting Scattering Losses with PSPICE

Note: This section presumes that the reader is familiar with basic electronic circuits. For those who are not, this section can be skipped without a loss of continuity.

Scattering losses occur primarily at the interface between layers. When an interface is encountered, some of the signal is reflected (scattered) away. The same phenomenon occurs in acoustics. When a sound wave encounters a change in media, for example, a wall, some of the sound is reflected off it. Whether acoustic or electromagnetic, the physics of reflection is the same. It is the change in the wave's velocity at the interface that gives rise to the reflection.

A reflection will always occur when a wave encounters an obstacle which causes its velocity to change. If the obstacle is normal (perpendicular) to the path of the wave, the magnitude of the reflected signal can be calculated from the relative velocities:

$$\Gamma = \frac{|v_2 - v_1|}{|v_1 + v_2|}$$

Where:

Γ = Reflection coefficient (varies between 0 and 1)

v_1 = Speed of the wave in medium 1

v_2 = Speed of the wave in medium 2

Note that if the velocities are the same, there is no reflection.

For example, in Figure 8 an electromagnetic wave is traveling in Stratum 2 and strikes the interface with Stratum 3. From Appendix A we know that:

$$v = \frac{c}{\sqrt{\kappa}}$$

Where:

c = Speed of light (3×10^8 m/sec)

κ = Relative permittivity

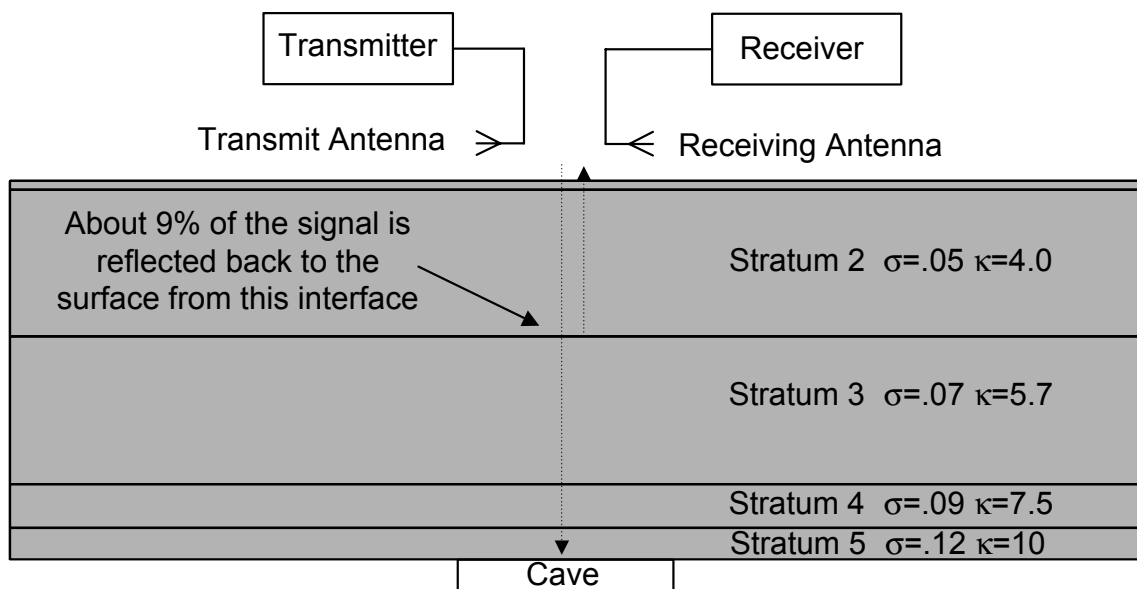


Figure 8: Velocity changes cause reflections. The change in velocity of the radar signal between Stratum 2 and 3 causes a reflection from their interface.

Therefore, the amount of signal reflected is:

$$\Gamma = \left| \frac{v_3 - v_2}{v_2 + v_3} \right|$$

$$v = \frac{c}{\sqrt{\kappa}}$$

$$\Gamma = \left| \frac{\frac{c}{\sqrt{\kappa_3}} - \frac{c}{\sqrt{\kappa_2}}}{\frac{c}{\sqrt{\kappa_2}} + \frac{c}{\sqrt{\kappa_3}}} \right|$$

$$\Gamma = \left| \frac{\frac{1}{\sqrt{\kappa_3}} - \frac{1}{\sqrt{\kappa_2}}}{\frac{1}{\sqrt{\kappa_2}} + \frac{1}{\sqrt{\kappa_3}}} \right|$$

$$\Gamma = \left| \frac{.42 - .5}{.5 + .42} \right| = .087$$

About 9% of the signal is reflected away.⁴

At Mersa/Wadi Gawasis there are many layers, and therefore many reflections to consider (Figure 9). Problems this complex are best solved through electronic computation, and for that purpose we used a program known as PSPICE.

PSPICE is an IBM-PC compatible version of SPICE, (Simulation Program for Integrated Circuits Emphasis). It is not a geophysical program, but rather software for simulating electronic circuits. It was originally developed at the Electronic Research Laboratory of the University of California at Berkeley in 1975. Using PSPICE, an electrical engineer can design and test a circuit without actually having to build it. Cadence Design Systems, Inc. has made a limited edition available at <http://www.electronic-lab.com/downloads/schematic/013/>. The Department of Electrical and Systems Engineering at the University of Pennsylvania has published an excellent tutorial on PSPICE entitled “PSPICE: A Brief Primer” and has made it available at <http://www.seas.upenn.edu/~jan/spice/PSpicePrimer.pdf>.

When we probe the subsoil electronically, we are, in fact, creating a kind of electronic circuit. We do so by coupling a signal to an antenna, which in turn couples it into the soil. The signal moves through the soil as it would through any electronic circuit, part of the signal being dissipated or scattered, and part of it returning to the surface. Since the soil functions as a kind of electronic circuit, we can use PSPICE to predict the results.

⁴ These formulas apply when the interface between layers as well as the surface is relatively horizontal. Since this is the case at Mersa/Wadi Gawasis, we will consider only this “normal incidence” case.

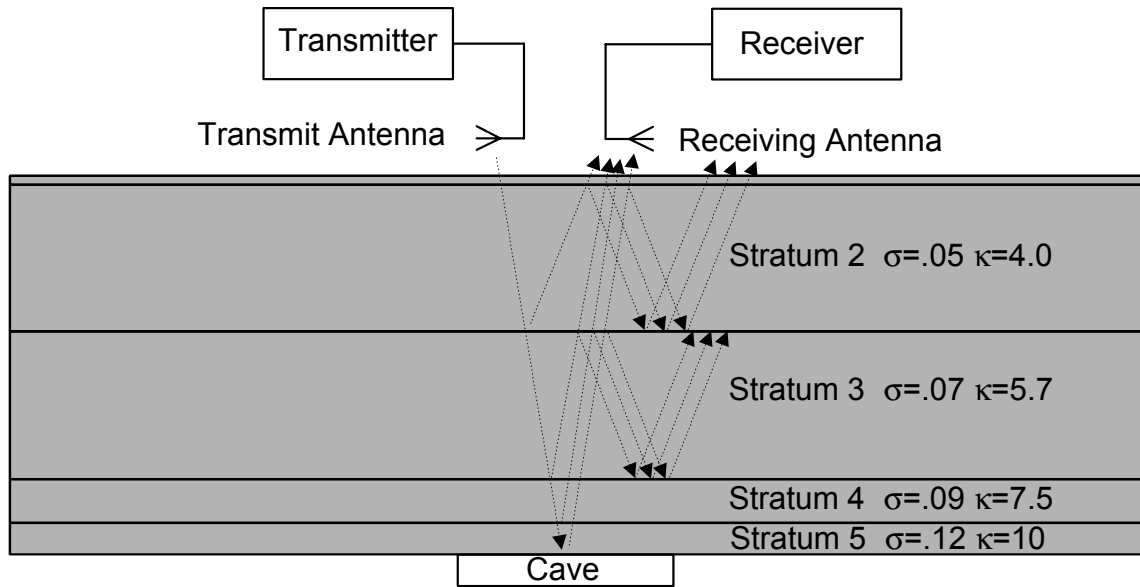


Figure 9: A more complete model of losses will include reflections from interfaces. When we include multiple reflections the model becomes computationally complex

In Figure 10, our PSPICE simulation circuit includes four cylindrical constructions known as coaxial transmission lines. A coaxial transmission line consists of a conductive cylinder with a wire down the center. The space between the cylinder (known as the “shield”) and the wire (“center conductor”) is filled with a medium (or “dielectric”). The characteristics of the coaxial transmission line are a function of its geometry, as well as the conductivity, permittivity and permeability of the medium used. In fact, we can fill a specially designed coaxial transmission line with the soil from a given stratum at Mersa/Wadi Gawasis, and any electrical signal we send through it will pass through it just as if it is were signal sent out from our radar down through the actual soil.⁵

In order to undertake the simulation, we need electrical models for the transmitter, the receiver and their antennas. The circuit that does this consists of a radio frequency (RF) source, two switches, one resistor and a voltage probe. The RF source produces a 200 MHz sine wave. The oscillator runs continuously, so we use a switch (U1) to cut off the signal after 7.5 nanoseconds, or one and one half cycles, to produce a “wavelet”. The transmit antenna has a “characteristic impedance” which is simulated by resistor R₁. The second switch has a function that will be explained below.

We use a second resistor, R₂, to simulate the cave. Our model assumes that the cave is air filled, and what we want to determine how much signal will be reflected off the roof of the cave. If we know the velocity of the wavelet in the stratum above the cave and the velocity of the wavelet in air, we can calculate the reflection using the formulas above. However, PSPICE does not let us program in velocities directly. Instead, we will use PSPICE’s ability to model impedances, which, it turns out, is the same thing.

Propagating electromagnetic waves have two components: an electric field and a magnetic field (Figure 11). The impedance of an electromagnetic wave is defined as the ratio of its electric field to its magnetic field at any one point in space. According to Kraus (Kraus 1992: 682), for the kind of materials we are dealing with ($\mu=\mu_0$), that ratio is equal to:

$$Z = \sqrt{\frac{\mu_0}{\epsilon}} = \sqrt{\frac{\mu_0}{\kappa\epsilon_0}}$$

Where:

Z = Wave impedance in ohms

In air, where $\epsilon=\epsilon_0$ and $\mu=\mu_0$ the wave impedance is:

$$Z_{air} = \sqrt{\frac{\mu_0}{\epsilon_0}} = \sqrt{\frac{4\pi \times 10^{-7}}{8.85 \times 10^{-12}}} = 377 \text{ ohms}$$

⁵ Creating an exact equivalence requires that the diameter of the shield must be 539 times the diameter of the center conductor.

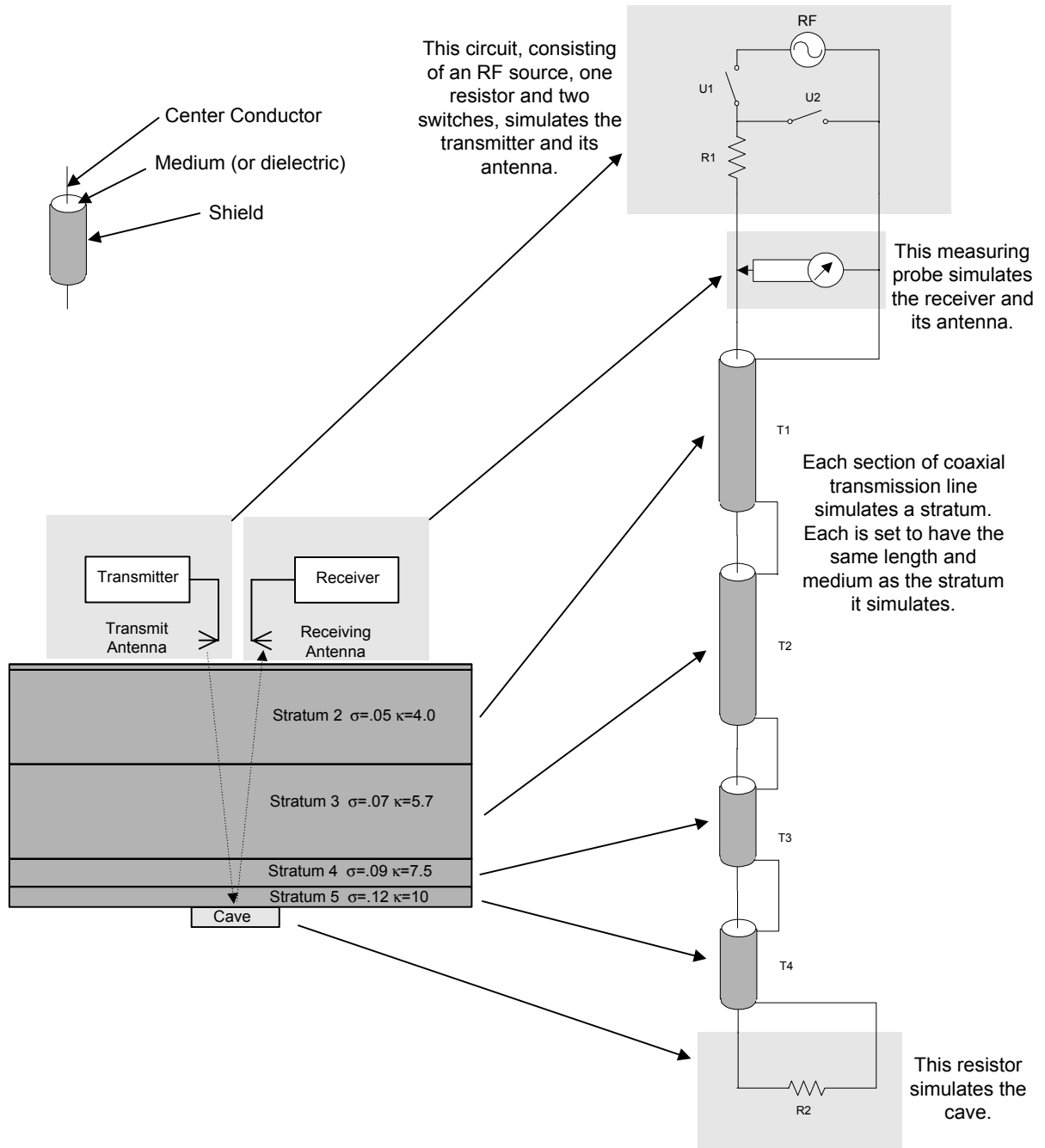


Figure 10: We can use PSPICE to predict scattering losses. Each stratum is modeled with a section of transmission line filled with a medium having the same properties as the soil we found at Mersa/Wadi Gawasis. The cave is simulated by a resistor. A combination of two switches, a resistor and a probe simulates the transmitter, receiver and their antennas.

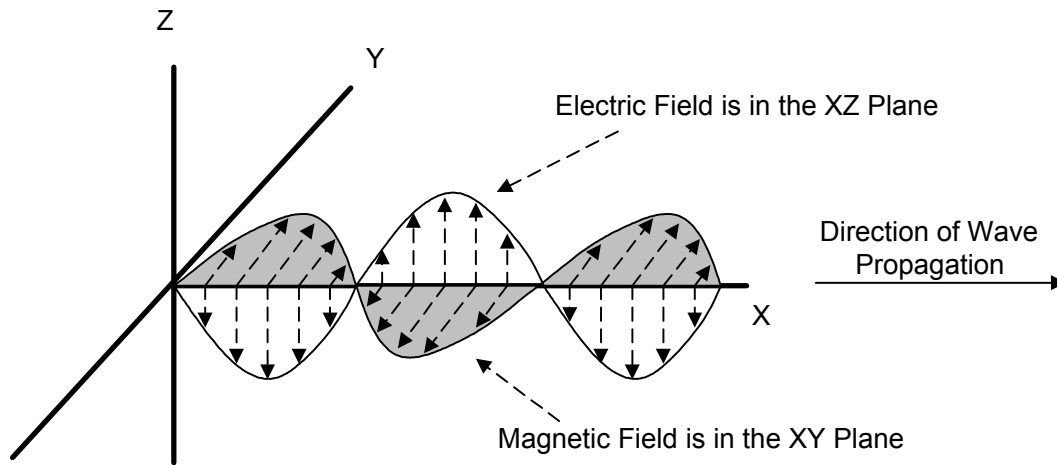


Figure 11: A propagating electromagnetic wave has two components: an electric field and a magnetic field, oriented at right angles to each other. The ratio of the amplitudes of the two fields is equal to the wave impedance.

Similarly, in other media where $\epsilon = \kappa \epsilon_0$ the wave impedance is:

$$Z = \sqrt{\frac{\mu_0}{\kappa \epsilon_0}} = \frac{377}{\sqrt{\kappa}}$$

$$v = \frac{c}{\sqrt{\kappa}}$$

$$Z = 377 \frac{v}{c}$$

Therefore, if we know the wave's velocity, we know its impedance as well.

Naturally, our cave is filled with air. To simulate our air-filled cave, we simply add a resistor at the end of our last transmission line equal to the wave impedance in air, 377 ohms.

Our model is almost complete. To finish it, we have to make sure that the wavelet does not return to the surface only to be reflected downward again. To prevent this, we can match the velocity (or impedance) of our simulated receiving antenna to the uppermost transmission line in Figure 10. This transmission line has an impedance equal to:

$$Z = \frac{377}{\sqrt{\kappa}} = \frac{377}{\sqrt{4}} = 188.5$$

Therefore, we set R_1 to 188.5 ohms. Finally, we add a second switch, U_2 , to close after switch U_1 opens in order to direct the returning signal to resistor R_1 .

Figure 12(a) shows the results of our simulation. The initial wavelet was detected at the probe (our simulated receiver) at the start of our simulation. Its amplitude was 0.5 Volts but little can be detected beyond that.

In order to detect all the reflections, we had to adjust the gain. Figure 12(b) shows the same results on a one millivolt scale, effectively applying a gain of 1000. The first reflection was from the Stratum 2-3 interface and was detected at the probe approximately 29 ns after transmission. Likewise, reflections from the other interfaces arrive back at the probe 64 and 72 ns after transmission. The reflection from the cave roof shows up after 82 ns. After that, we can detect only small reflections caused by reverberations between strata.

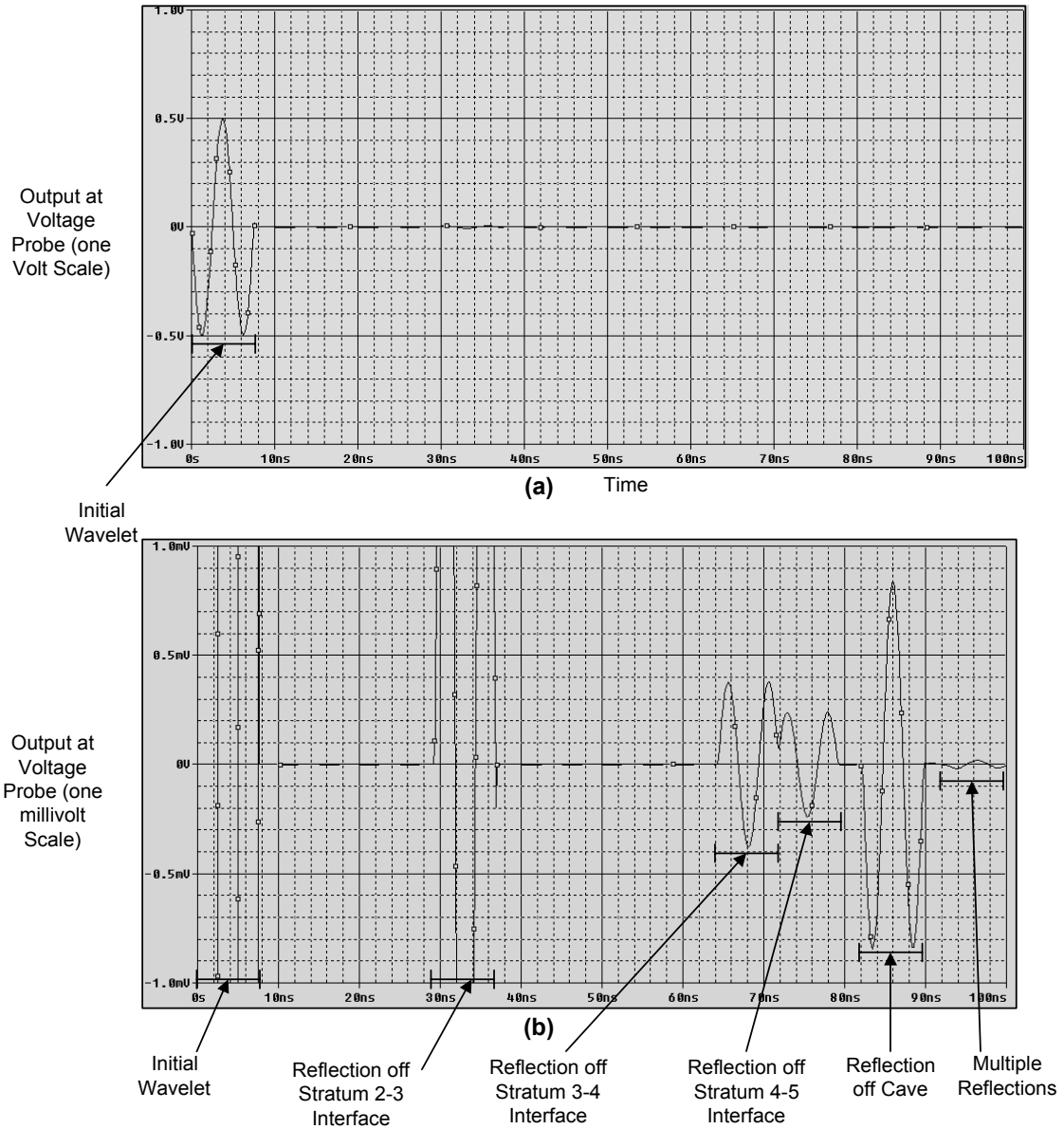


Figure 12: The results of our simulation. In (a), the voltage probe (our simulated receiver) detects the initial wavelet immediately after transmission. In (b) the results are magnified 1000 times. The wavelet reflects off interfaces between strata, finally reflecting off the cave roof and returning to the receiver after approximately 82 nanoseconds. The peak amplitude of the reflection off the cave is 0.84 millivolts. The initial wavelet was one half volt and therefore just over one part in one thousand of the initial signal returns.

The amplitude of the reflection from the cave is what is most critical to our analysis. Our probe initially measured an outgoing signal of 0.5 volts. The signal received back from the cave was 0.84 millivolts. The total of our scattering and absorption losses is:

$$Loss(dB) = -20 \log \left(\frac{S_{received}}{S_{transmitted}} \right)$$

$$S_{received} = 0.84mV$$

$$S_{transmitted} = 0.5V$$

$$Loss(dB) = 55.5dB$$

Our numerical analysis, which considered absorption losses alone, predicted a loss of 49.7dB. Our PSPICE simulation includes scattering losses as well and predicts 55.5dB, or an additional loss of 5.8dB due to scattering.

A loss of 55.5dB would be tolerable. However, our PSPICE model does not include antenna, transmission or spreading losses. For accurate prediction of these losses we have to turn to a more sophisticated tool, a full electromagnetic wave simulator.

VI: Predicting Losses with Electromagnetic Wave Simulation

A full electromagnetic simulator solves Maxwell's Equations directly, generating a matrix of predicted electric and magnetic fields anywhere within a chosen volume. Unfortunately, Maxwell's Equations are very complex, and even modern computers solve them slowly. Furthermore, electromagnetic wave simulators are difficult to use and considerable knowledge of electromagnetic wave theory is needed to reliably interpret results. Therefore, full electromagnetic wave simulation is rarely used in archaeological geophysics. However, the caves at Mersa/Wadi Gawasis are so deep that using numerical analysis and PSPICE alone is not sufficient to make predictions.

Here, we will use GprMax2D, freeware written by Dr. Antonis Giannopoulos of the University of Edinburgh <http://www.gprmax.org/index.php>. Although designed specifically for GPR applications, this program is only a "computational engine." In other words, it was designed to be inserted into other applications which provide for user-friendly input and output. Nevertheless we are able, with some difficulty, to use it to predict how well the radar will work.

To use the software, we first draw models of the volume of soil we want to simulate (Figure 13). We will examine two volumes, one with and one without the cave. We will set the X and Y boundaries of our volume at 10 by 10 meters, the Z boundaries at infinity, and include six air and soil strata. We will place our transmitting and receiving antennas just over the surface of the first soil layer. In Stratum 5 of our second model we have carved out a 4 by 2 meter cave.

We provide all this information to GprMax2D in the form of a .txt file (Appendix C). The output generated by GprMax2D is also a .txt file which the reader can find at <http://www.DashFoundation.org/HowDeep/GprMax2d.zip>. To produce a useful numerical and graphical output, we used Microsoft Excel to generate the plots shown in Figure 14.

We ran the caveless model first. Only visible in Figure 14(a) is the transmit wavelet as it was received at the receive antenna immediately after transmission. In order to see more detail, we need to increase the gain and in Figure 14(b) we have effectively increased the gain by 1000 (60 dB). We can clearly see the transmitted signal and a first reflection from the interface between Strata 2 and 3. We can also see weaker reflections from the other interfaces.

In Figure 14(d) we have arranged to keep all the returning signals on screen by increasing the gain with time. We do this by applying the gain curve in Figure 14(c). In Figure 14(d) we can just detect reflections from all the interfaces of the caveless model.

Figure 15 compares the caveless model with the cave model. We applied the gain curve from Figure 14(c) to produce both Figures 15(a) and (b). In Figure 15(b), both the roof and the floor of the cave produced marked reflections. These are followed by reverberations caused by signals bouncing between the roof and floor.

Unfortunately, all these signals are weak. In Figure 15(b), we have also plotted the “60dB” and “80dB” noise thresholds. If the noise threshold is 60dB below our transmitted signal (a factor of 1000) the noise will be strong enough to mask the reflections from the cave entirely. If the noise is threshold 80dB below our transmitted signal (a factor of 10,000), we should just be able to detect the cave.

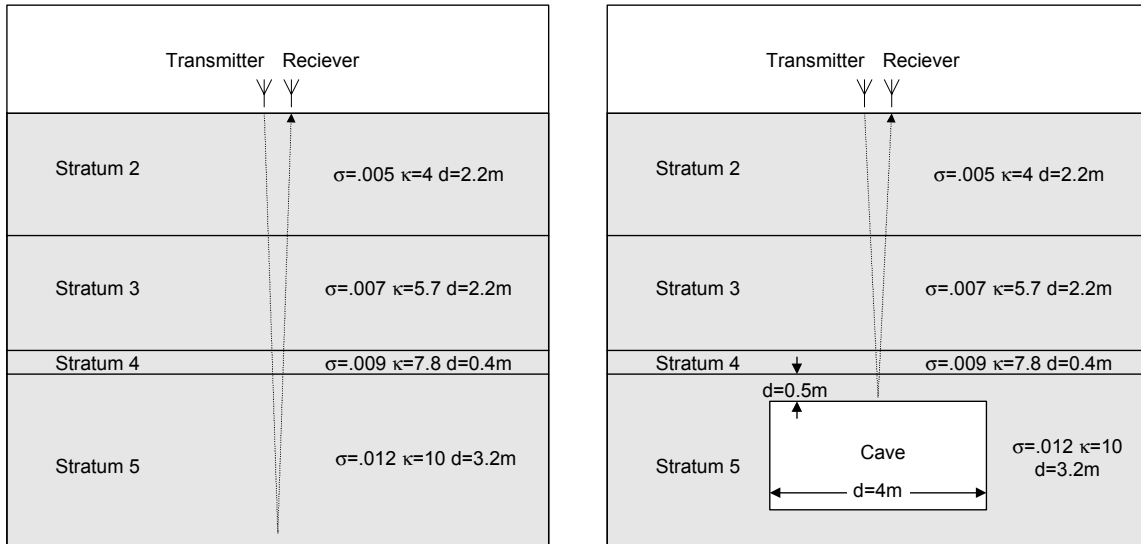


Figure 13: To use an electromagnetic wave simulator such as GprMax2D, we construct models of the volume we want to simulate. We have constructed two such volumes, one with and one without the cave.

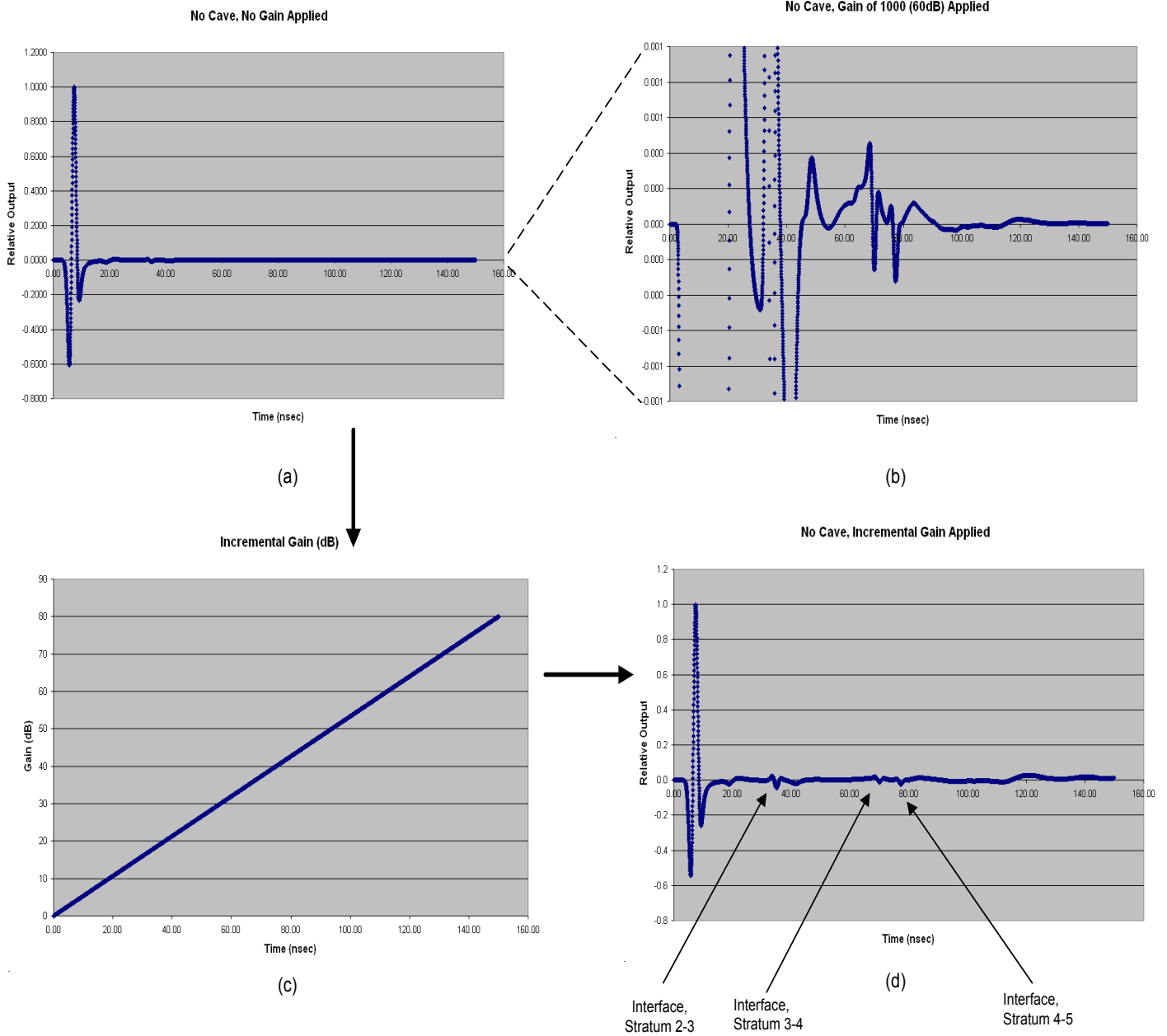
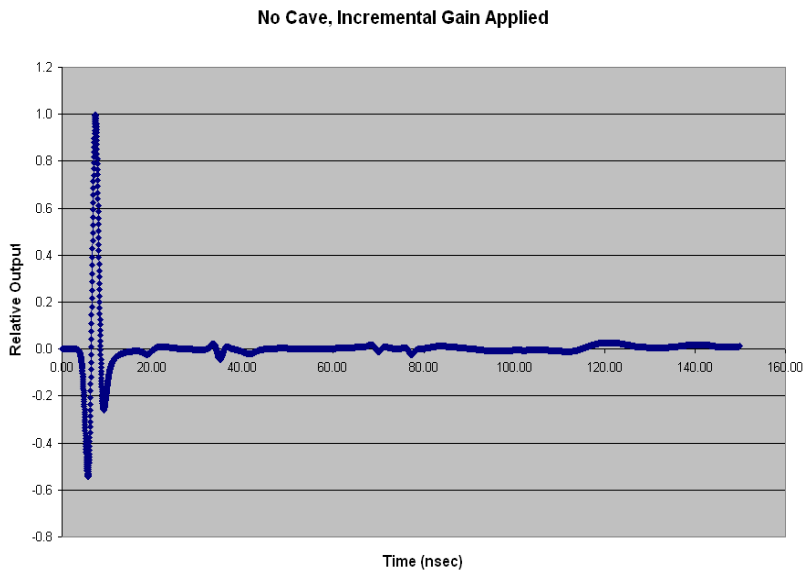
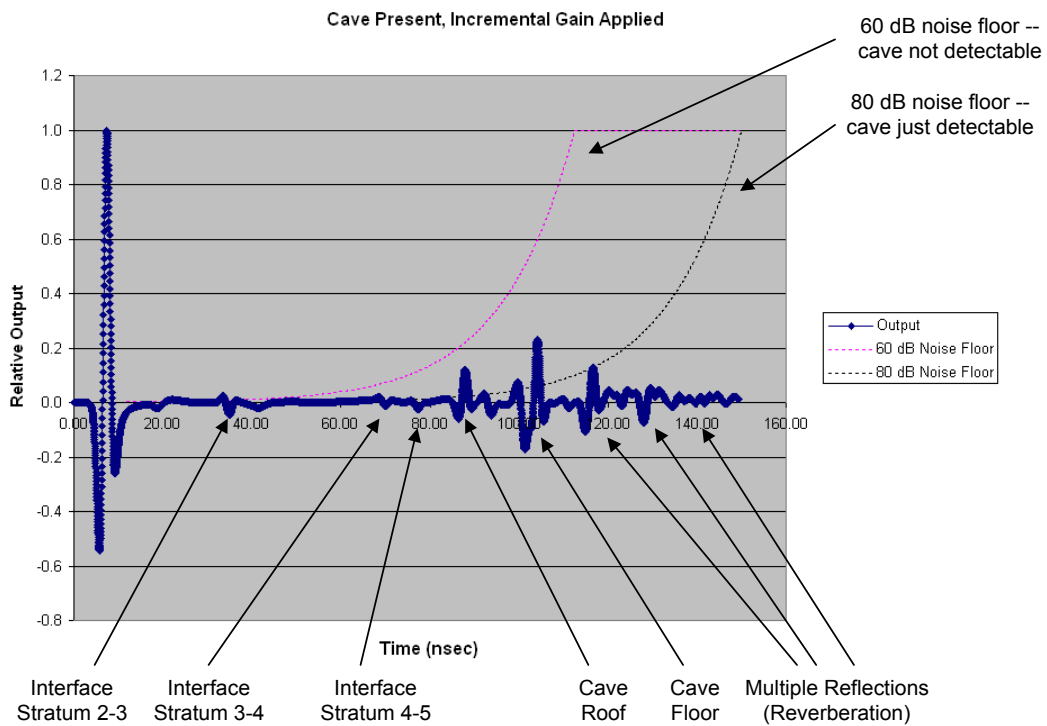


Figure 14: We show the output provided by GprMax2D without the cave present at (a). In order to see the reflections, we need to provide gain. We do so at (b) by magnifying the area around the x axis, effectively applying a gain of 1000. However, to better see the results, it is best to apply a gain that increases with time. The gain curve at (c) is applied to the plot at (a) to produce the result at (d).



(a)



(b)

Figure 15: We show results without the cave present (a) and with the cave present (b). We applied incremental gain (Figure 14(c)) to the output of our simulation to create both traces. Whether the cave will be detectable depends on the noise floor. The dotted lines in (b) demark the 60 dB and 80 dB noise floors.

VII: The 2006/2007 Field Season at Mersa/Wadi Gawasis

In December of 2006 and January of 2007, Mr. Benjamin Vining of Boston University, with support from the Glen Dash Charitable Foundation, undertook a ground penetrating radar study at Mersa/Wadi Gawasis. The purpose of the study was to determine whether additional caves could be detected using radar. To conduct the study, Mr. Vining used a Geophysical Survey Systems (GSSI) SIR-2000 radar system with a 200 MHz antenna. The data he collected can be found at <http://www.DashFoundation.org/HowDeep/RadarFiles.zip>.

Figure 16 shows the location of six transects Mr. Vining surveyed. Transects 1 and 2 run roughly south-north and are separated by approximately 5 meters. Transects 3 and 4 run east-west along a common pathway, as do Transects 5 and 6.

The SIR-2000 system is designed to automatically transmit wavelets into the ground as its “radar sled,” the box containing its antennas, is pulled along a pathway. The interval between transmissions is adjustable by the operator. For example, in Figure 17(a) we have simulated the transmission of one wavelet every 3 meters along Transect 1. The recorded traces are placed side by side for convenience, creating what is known as a “*wiggle trace*” plot. In Figure 17(b) we have decreased the interval to one trace every 30 centimeters. Note that the combination of traces begins to look like a profile of the subsurface.

We can discern more detail by color encoding the data. In Figure 18, we have transformed each trace by assigning different colors to portions of it depending on its amplitude at any given time. The result is known as a *radargram*.

We show the radargram for Transect 1 at the bottom of Figure 18. We can clearly see the interface between Stratum 2 and 3. Beneath this, we can also see some reflections at approximately 80 nanoseconds, reflections which are well correlated with the location of some of the known caves.

We processed this data using the “GPR-Slice” software written by geophysicist Dean Goodman. The software takes two or more nearby radar profiles and combines them to produce a map of reflected energy. It does this by “slicing” horizontally across individual radar profiles at a common depth, then “gridding” vertically to create individual volume units. The amount of energy within each volume unit is then calculated by squaring the amplitude of the signals each volume contains. The resulting map identifies the sources of reflected energy from the subsurface.

Figure 19 contains the reflected energy map for Transect Pair 1-2.⁶ The areas in orange and red exhibited the most reflected energy from any given strata and the areas in green and blue relatively less. In Figure 20, we have added the locations of known caves. The locations of

⁶ In processing this data, we followed the algorithm described in Appendix D.

Caves 1, 2, 3, 4 and 7 are well correlated with the map of reflected energy. However, there were also strong reflections detected at depths where no caves were found. In some cases, the reflections were from locations near to the surface.

Daniels has offered an explanation:

“Water movement through sandy soils is not uniform and is strongly influenced by soil layering. Coarser or finer textural layers redirect and concentrate water movement into preferential pathways. The pathways move water and solutes laterally over restrictive layers and downward through discontinuities in these strata. These flow paths or *fingers* occupy a small part of the soil but account for most of the water movement and chemical transport.” (Daniels 2004: 105)

The water movement Daniels describes is probably the cause of the patterns of reflected energy we find in Figure 20. Water has percolated down from the surface, finding its way through the less restrictive rock and along fissures. The water movement left behind more porous, less homogenous rock, with many surfaces to reflect radar energy. The ancient cave builders apparently took advantage of such places for their caves. Partially eroded rock, naturally, is easier to carve. That is fortunate for us, because it is easier to find the fingers than the caves themselves. In looking for more caves, we can start by looking for the “fingers” Daniels describes.

In Figure 21, we have plotted the returned energy profiles for the other two pairs of transects, 3-4 and 5-6. These run roughly east-west, and display evidence of the same kind of layering and fingers we found in the north-south pair 1-2. That means that the effect Daniels describes occurs not only along the edge of the terrace, but throughout its volume. Note also that Cave 6, which was not detected along Transects 1-2, appears clearly in the data from Transects 5-6. The cave may have been too close to the edge of the terrace to have been detected in Transects 1-2.

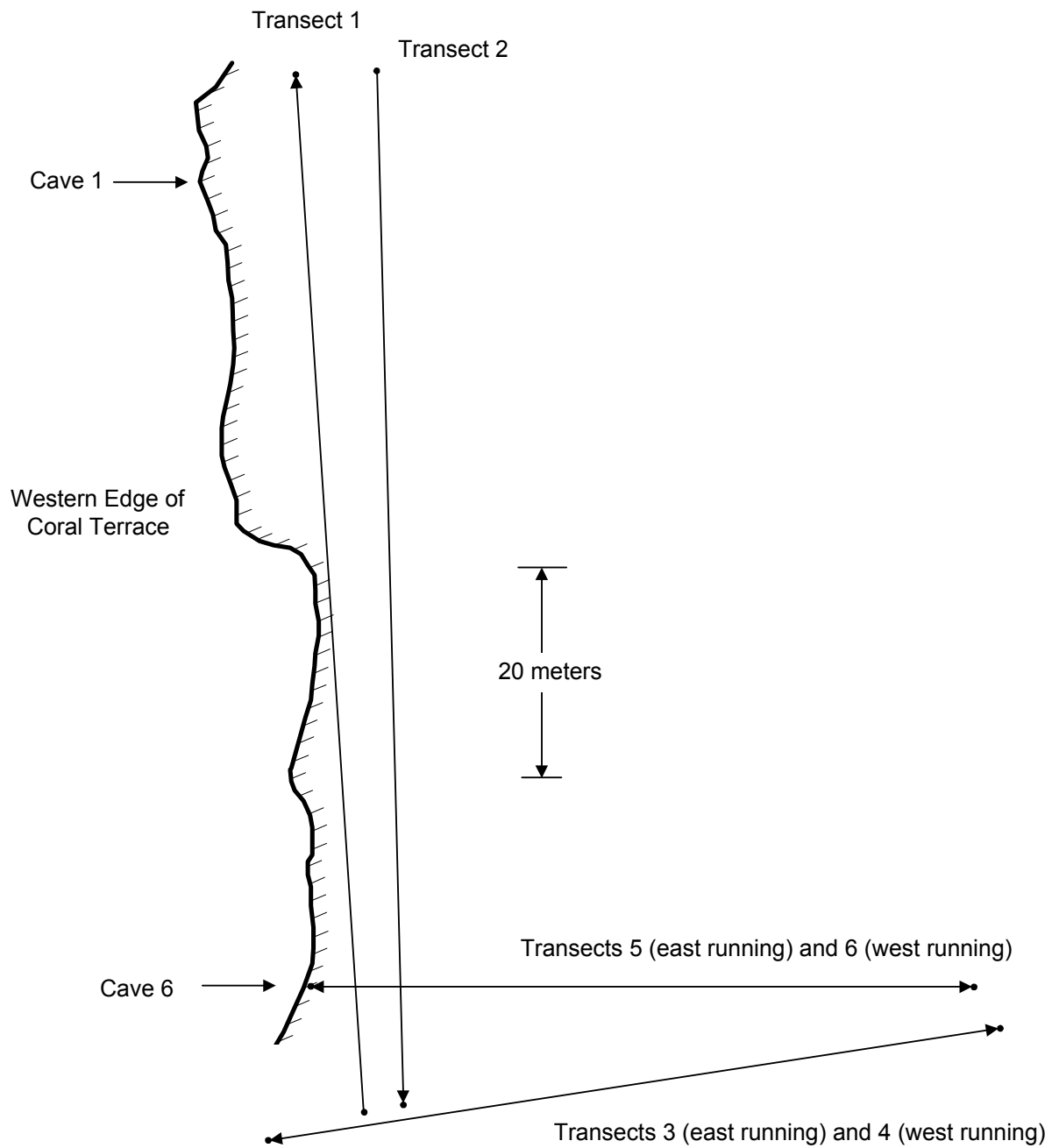
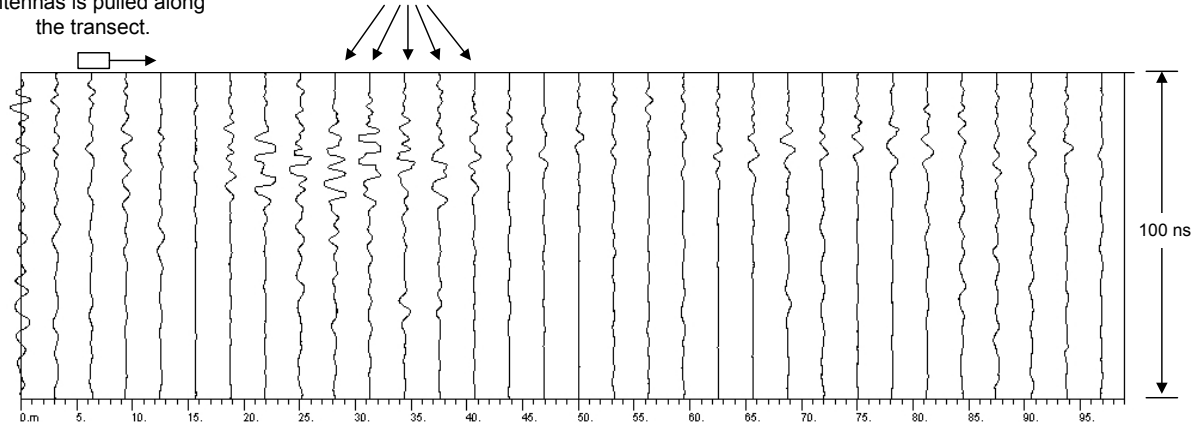


Figure 16: During a 2006-2007 field season, Mr. Benjamin Vining conducted radar surveys along six transects near the western edge of the coral terrace. Transects 1 and 2 ran south and north. Transects 3 and 4 ran roughly east and west. Two more east-west transects, 5 and 6, were run just to their north. (Credit: Vining 2006-2007)

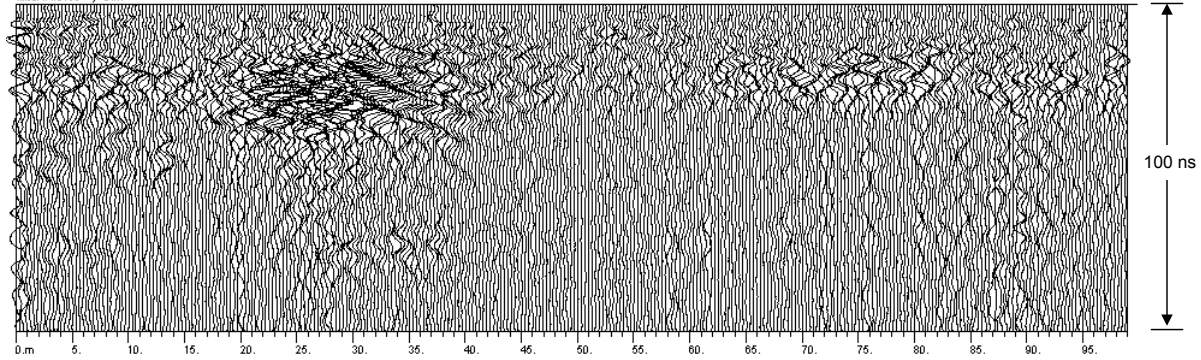
The radar sled containing transmitting and receiving antennas is pulled along the transect.

In this example, the radar sends out a wavelet every 3 m.



(a)

Here, the radar sends out a wavelet every 30 cm, frequently enough to form an image of the subsurface.



(b)

Figure 17: We record a subsurface radar profile by dragging a radar sled along a predetermined pathway. The radar can be adjusted to transmit a radar pulse, or wavelet, at intervals as it is dragged along. We record the received signal, or trace, at each location. At the top (a), the interval between transmissions is about 3 meters. At the bottom (b), the interval is reduced to about 30 cm and an image begins to form.

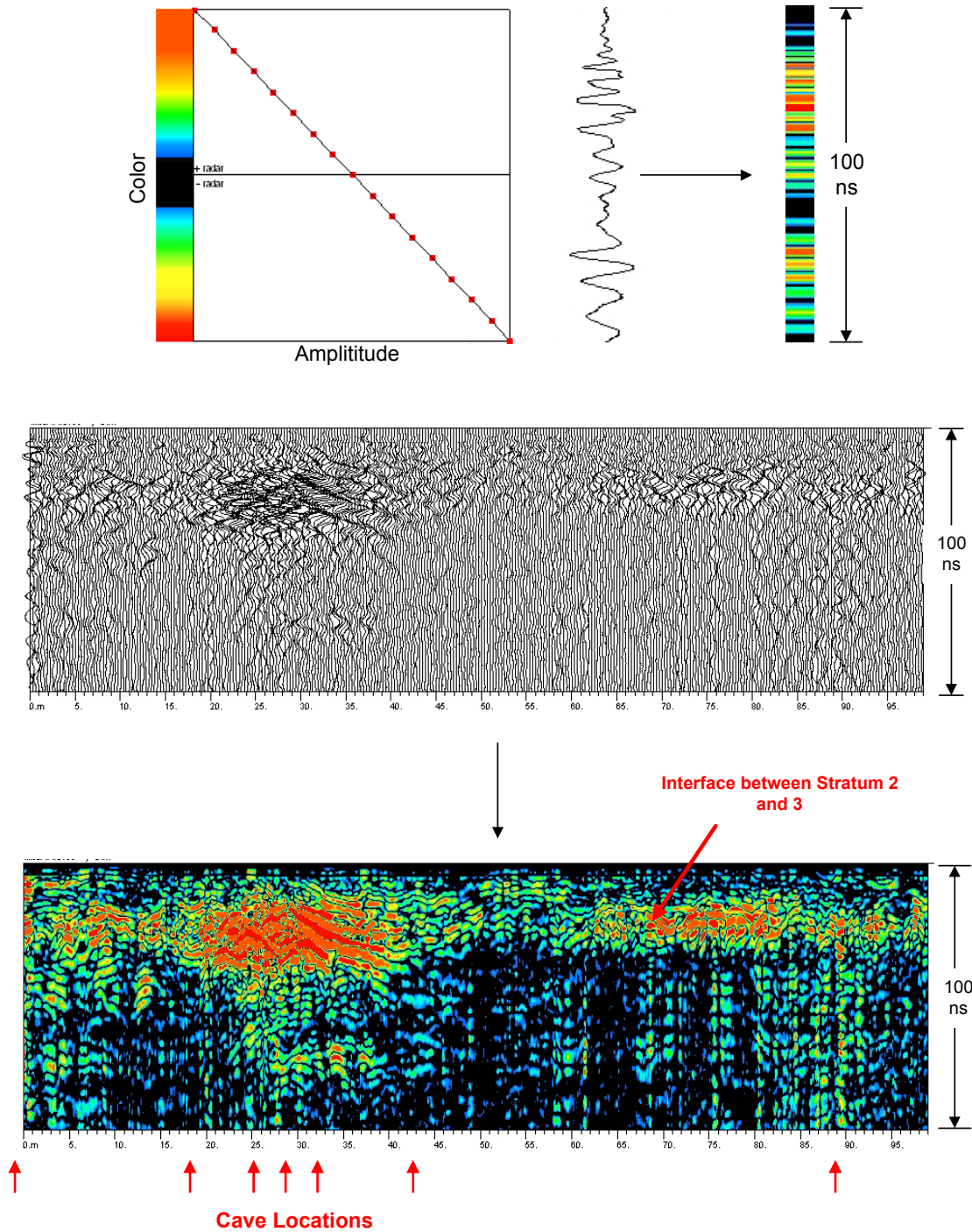
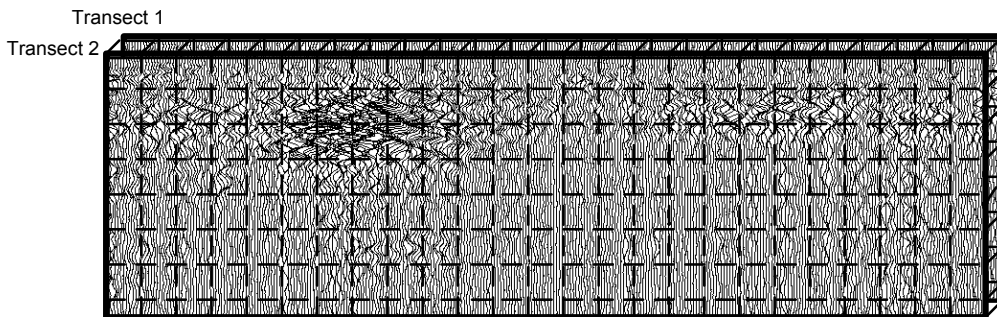
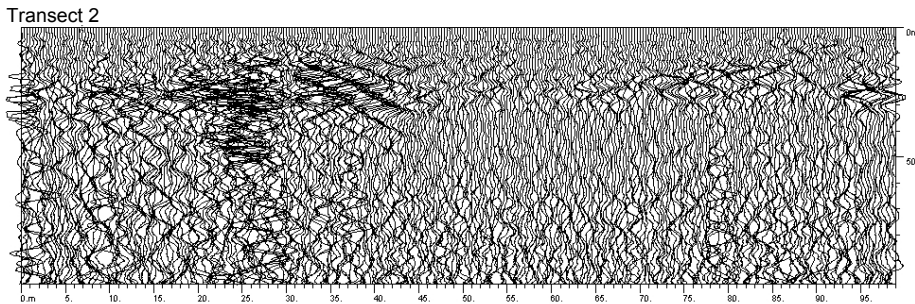
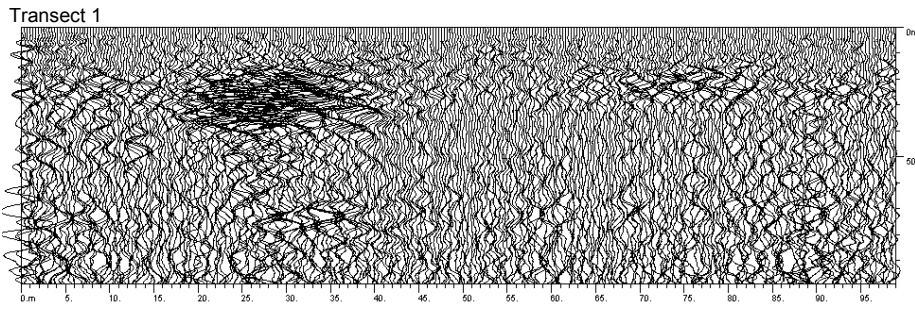
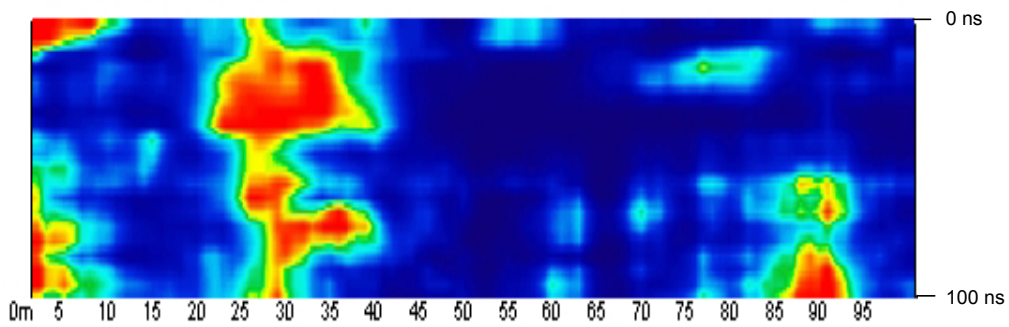


Figure 18: An alternative presentation to the wiggle trace plot of Figure 17 is the radargram. We produced the radargram at the bottom by encoding each trace as a series of colored bands, as shown at the top. The bands represent the amplitude of a given trace at a given time. Placed side by side, these colored bands convert a wiggle trace plot to a radargram. Shown here is the radargram for Transect 1. The interface between Stratum 2 and 3 is clearly visible at approximately 25 nanoseconds, as is a hint of the caves at about 80 nanoseconds.



Slicing across radar profiles and gridding creates small volume units ...



... and squaring the returns creates this map of reflected radar energy.

Figure 19: We can extract more detail by combining the information from two or more parallel transects using GPR Slice. The software electronically places two or more transects side by side and then slices and grids these to create small volume units. It then calculates the total energy reflected from each unit. The result is the profile shown at the bottom, which is a map of the relative reflected energy from a vertical slice of the subsurface.

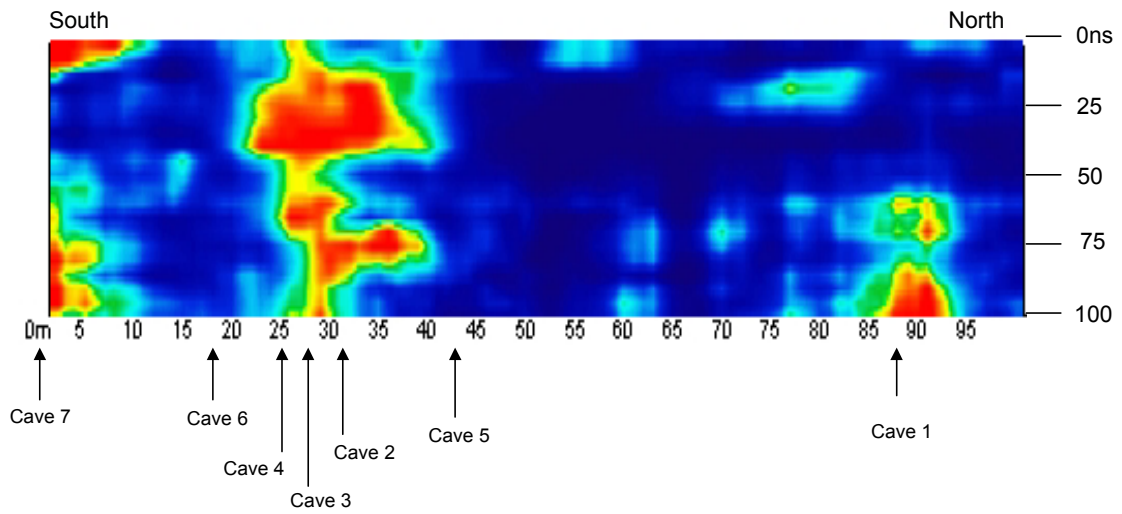


Figure 20: The reflected energy profile along north-south Transects 1 and 2 correlates well with the locations of Caves 1, 2, 3, 4 and 7.

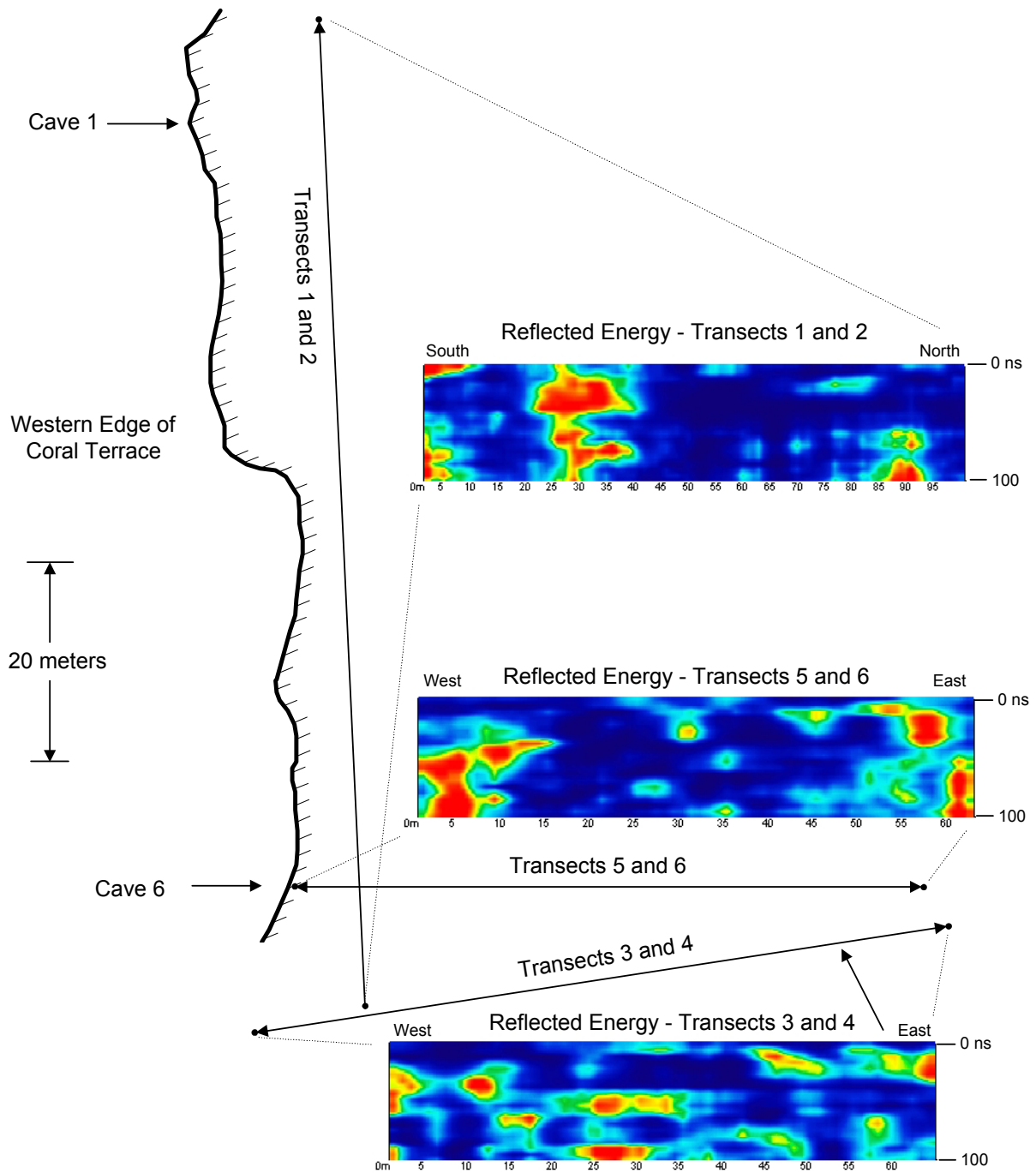


Figure 21: The map of reflected energy for these three pairs of transects shows areas where the rock is less homogeneous and therefore more reflective. This heterogeneity is likely caused by the movement of water from the top of the terrace either downward or preferentially across certain soil layers.

VIII. Conclusions

Mersa/Wadi Gawasis, with its exposed profile and caves, offers a unique opportunity to combine geophysical experimentation with archaeological investigation. By measuring the individual strata, we were able to estimate the conductivity and permittivity of each. Using this data, we were able to predict absorption losses using a numerical analysis, scattering losses using PSPICE, and the overall shape and amplitude of the return trace with Gpr2DMax.

Numerical analysis is quick; it can be performed in the field with pencil and paper. Our numerical analysis revealed we could expect almost 50 dB of loss due to absorption alone. With an expected noise threshold of 60 to 80 dB, this left us only a few dB to spare.

PSPICE is a program that can predict both absorption and scattering losses. It is fast, easy to use, and widely available. PSPICE predicted total losses of at least 55.5 dB. With such a narrow margin, we had to employ a full electromagnetic wave simulator, GprMax2D to better predict the results.

Full wave electromagnetic simulators are difficult to program and interpret, and are rarely used for archaeological predictions. However, with some difficulty we were able to show that the caves would be detectable if our noise threshold was 80 dB below our transmitted signal, but not if it was only 60 dB. The noise threshold at any particular location depends on factors such as local electrical noise and is impossible to predict.

Our field study revealed that the ancient cave builders carved their caves into relatively soft rock. This rock had been weakened by water transport from the top of the terrace. The water transport produced porous “fingers” vertically throughout the terrace, and horizontally along preferential rock layers. The radar readily detected these fingers. While our simulations indicated that the caves would have been difficult to detect, the presence of these fingers made the job much easier.

Detection of additional caves is certainly feasible. Surveyors could pull the radar along the edges of the terrace and process the data using GPR Slice. The results should indicate the locations where the ancient Egyptians could have carved out caves, if not the caves themselves.

Appendix A: A Primer on the Propagation of Electromagnetic Signals through Soils

Mathematically, an electromagnetic wave transmitted into the soil has the following characteristics (Kraus 1992: 549):

$$E(x) = E_0 e^{-\gamma x}$$

Where:

- $E(x)$ = Electric field at point x (Volts/m)
- E_0 = Electric field at the surface ($x = 0$)
- γ = Propagation constant
- x = Distance from the surface in meters

The “propagation constant” gamma (γ) is equal to:

$$\gamma = \sqrt{j\omega\mu\sigma - \omega^2\mu\epsilon}$$

Where:

- ω = Frequency in radians per second ($=2\pi f$)
- f = Frequency in Hertz
- μ = Permeability in Henries per meter
- σ = Conductivity in Siemens per meter
- ϵ = Permittivity in Farads per meter

The propagation constant gamma has real and imaginary parts. These are equal to:

$$\text{Re } \gamma = \text{Re } \sqrt{j\omega\mu\sigma - \omega^2\mu\epsilon}$$

$$\text{Im } \gamma = \text{Im } \sqrt{j\omega\mu\sigma - \omega^2\mu\epsilon}$$

If we call the real part alpha (α) and the imaginary part beta (β) then we have:

$$E(x) = E_0 e^{-\gamma x}$$

$$\gamma = \alpha + j\beta$$

$$E(x) = E_0 e^{-\alpha x} e^{-j\beta x}$$

This equation states that the amplitude of the electromagnetic wave falls off exponentially with increasing x . Furthermore, since $E(x)$ goes through one full cycle when $\beta x = 2\pi$, the wave also has a wavelength (λ) equal to $2\pi/\beta$.

If we want to know how far away a target can be and still be detectable, we need to solve for α . Over a distance of $x=1/\alpha$ the amplitude of the signal falls by $1/e$, or to .368 of its original value. Modern subsurface radars can detect reflected signals that are between 1/1000 (60dB) and 1/10,000 (80dB) of their original values. If we want to know the distance x over which the signal will fall to .001 of its original value, then:

$$\begin{aligned} .001E_0 &= E_0 e^{-\alpha x} \\ .001 &= e^{-\alpha x} \\ \ln(.001) &= \ln(e^{-\alpha x}) \\ -6.91 &= -\alpha x \\ x &\approx 7/\alpha \end{aligned}$$

If we call $1/\alpha$ delta (δ), then we can say that the signal will fall by a factor of 1000 over a distance of about 7δ . To detect the cave, the signal must reach the cave and be reflected back to the surface. Therefore, to be detectable, the cave must lie no more than 3.5δ below the surface. If our radar is more sensitive and can detect one part in ten thousand of the transmitted signal, then the depth we can reach will be approximately 4.5δ

As for the length of time that will take, that depends on the wave's velocity. Velocity equals the wavelength times the frequency;

$$v = f\lambda$$

Where:

$$\begin{aligned} \lambda &= \text{Wavelength in meters} \\ f &= \text{Frequency in Hertz} \end{aligned}$$

But we also know that:

$$\begin{aligned} \lambda &= 2\pi / \beta \\ \text{And :} \\ f &= \omega / 2\pi \\ \text{Therefore :} \\ v &= \omega / \beta \end{aligned}$$

To calculate the velocity we need to know the frequency in radians ($\omega=2\pi f$) and beta, β , the imaginary part of the propagation constant.

We have prepared an Excel spreadsheet which allows us to calculate how deeply we will be able to see into particular soils. For example, if we use a 50 MHz radar over a bed of uniform soil with a permeability equal to a vacuum ($\mu=\mu_0=4\pi \times 10^{-7}$), relative permittivity of 4 and conductivity of .010 Siemens per meter, we can expect to see at least 3.5δ down or 4.02 meters (Table 2, fourth line). Our signal will have a wavelength of 2.77 meters in the soil and will travel at a velocity of 1.38×10^8 meters per second, less than one half that of the speed of light.

We have plotted some of the data from Table 2 in Figure 22. Clearly, the depth we can observe rises with permittivity and falls with conductivity. (The permeability (μ) is assumed to be uniform over the soil volume and equal to the permeability of air.) However, the depth of observation is generally not a function of the transmitted frequency except in relatively conductive soils.

Using some common assumptions, we can simplify the equations somewhat. We will start with the equations for depth. The observable depth is between 3.5δ and 4.5δ , and $\delta=1/\alpha$ so:

$$\alpha = \text{Re } \gamma = \text{Re } \sqrt{j\omega\mu\sigma - \omega^2\mu\epsilon}$$

$$\alpha = \text{Re } \sqrt{-\omega^2\mu\epsilon} \sqrt{1 - \frac{j\sigma}{\omega\epsilon}}$$

Now let us assume that the term $\sigma/\omega\epsilon$ is small, that is $\sigma \ll \omega\epsilon$. In that case, since:

$$\sqrt{1-\theta} = \left(1 - \frac{\theta}{2}\right)$$

where:

$$\theta \ll 1$$

Then:

$$\alpha = \text{Re } \sqrt{-\omega^2\mu\epsilon} \left(1 - \frac{j\sigma}{2\omega\epsilon}\right) = \text{Re } j\sqrt{\omega^2\mu\epsilon} \left(1 - \frac{j\sigma}{2\omega\epsilon}\right) = \text{Re } \left[j\sqrt{\omega^2\mu\epsilon} + \frac{\sigma}{2} \sqrt{\frac{\mu}{\epsilon}} \right]$$

And where $\mu=\mu_0$:

$$\alpha = \frac{\sigma}{2} \sqrt{\frac{\mu_0}{\kappa\epsilon_0}} = \frac{188.5\sigma}{\sqrt{\kappa}}$$

The observable depth therefore is approximately:

$$\frac{.019\sqrt{\kappa}}{\sigma} > \text{Depth} > \frac{.024\sqrt{\kappa}}{\sigma}$$

Freq (Hz)	μ	σ	κ	ϵ	ω	$Re[\gamma^2]$	$Im[\gamma^2]$	γ	$Re[\gamma]$	δ (m)	$\delta\delta$ (m)	3.5δ (m)	4.5δ (m)	λ (m)	β	Velocity (m/sec)	Return Time (ns)
5.00E+07	1.26E-06	0.001	4	3.54E-11	3.14E+08	-4.39	0.39	9.41099857107141E-002+2.09746167243669i	0.09	10.63	74.38	37.19	47.82	3.00	2.10	1.50E+08	497
5.00E+07	1.26E-06	0.003	4	3.54E-11	3.14E+08	-4.39	1.18	0.280122433498797+2.11399085988557i	0.28	3.57	24.99	12.49	16.06	2.97	2.11	1.49E+08	168
5.00E+07	1.26E-06	0.007	4	3.54E-11	3.14E+08	-4.39	2.76	0.631391637019026+2.1884113363872i	0.63	1.58	11.09	5.54	7.13	2.87	2.19	1.44E+08	77
5.00E+07	1.26E-06	0.010	4	3.54E-11	3.14E+08	-4.39	3.95	0.870029694708021+2.26879713672337i	0.87	1.15	8.05	4.02	5.17	2.77	2.27	1.38E+08	58
5.00E+07	1.26E-06	0.015	4	3.54E-11	3.14E+08	-4.39	5.92	1.22092726453866+2.42510869101249i	1.22	0.82	5.73	2.87	3.69	2.59	2.43	1.30E+08	44
5.00E+07	1.26E-06	0.025	4	3.54E-11	3.14E+08	-4.39	9.87	1.79047712906212+2.75613808210419i	1.79	0.56	3.91	1.95	2.51	2.28	2.76	1.14E+08	34
5.00E+07	1.26E-06	0.001	9	7.97E-11	3.14E+08	-9.88	0.39	6.27907105126332E-002+3.14365112944649i	0.06	15.93	111.48	55.74	71.67	2.00	3.14	9.99E+07	1116
5.00E+07	1.26E-06	0.003	9	7.97E-11	3.14E+08	-9.88	1.18	0.188073309422831+3.14864595025557i	0.19	5.32	37.22	18.61	23.93	2.00	3.15	9.98E+07	373
5.00E+07	1.26E-06	0.007	9	7.97E-11	3.14E+08	-9.88	2.76	0.435463004751669+3.17304708109585i	0.44	2.30	16.07	8.04	10.33	1.98	3.17	9.90E+07	162
5.00E+07	1.26E-06	0.010	9	7.97E-11	3.14E+08	-9.88	3.95	0.616296196056028+3.20287694918438i	0.62	1.62	11.36	5.68	7.30	1.96	3.20	9.81E+07	116
5.00E+07	1.26E-06	0.015	9	7.97E-11	3.14E+08	-9.88	5.92	0.905249226630447+3.27079132820462i	0.91	1.10	7.73	3.87	4.97	1.92	3.27	9.60E+07	81
5.00E+07	1.26E-06	0.025	9	7.97E-11	3.14E+08	-9.88	9.87	1.42924643956892+3.45273009882961i	1.43	0.70	4.90	2.45	3.15	1.82	3.45	9.10E+07	54
5.00E+07	1.26E-06	0.001	16	1.42E-10	3.14E+08	-17.56	0.39	4.70994550405219E-002+4.19096331055128i	0.05	21.23	148.62	74.31	95.54	1.50	4.19	7.50E+07	1983
5.00E+07	1.26E-06	0.003	16	1.42E-10	3.14E+08	-17.56	1.18	0.141227115968627+4.19307765370576i	0.14	7.08	49.57	24.78	31.86	1.50	4.19	7.49E+07	662
5.00E+07	1.26E-06	0.007	16	1.42E-10	3.14E+08	-17.56	2.76	0.328707384986223+4.20357034634444i	0.33	3.04	21.30	10.65	13.69	1.49	4.20	7.47E+07	285
5.00E+07	1.26E-06	0.010	16	1.42E-10	3.14E+08	-17.56	3.95	0.468112905474654+4.21676236038904i	0.47	2.14	14.95	7.48	9.61	1.49	4.22	7.45E+07	201
5.00E+07	1.26E-06	0.015	16	1.42E-10	3.14E+08	-17.56	5.92	0.696963304026529+4.24825999191215i	0.70	1.43	10.04	5.02	6.46	1.48	4.25	7.40E+07	136
5.00E+07	1.26E-06	0.025	16	1.42E-10	3.14E+08	-17.56	9.87	1.13650810857308+4.34207390455001i	1.14	0.88	6.16	3.08	3.96	1.45	4.34	7.24E+07	85
2.00E+08	1.26E-06	0.001	4	3.54E-11	1.26E+09	-70.25	1.58	9.41989100810438E-002+8.38192662110256i	0.09	10.62	74.31	37.16	47.77	0.75	8.38	1.50E+08	496
2.00E+08	1.26E-06	0.003	4	3.54E-11	1.26E+09	-70.25	4.74	0.282454231937253+8.38615530741153i	0.28	3.54	24.78	12.39	15.93	0.75	8.39	1.50E+08	165
2.00E+08	1.26E-06	0.007	4	3.54E-11	1.26E+09	-70.25	11.05	0.657414769972446+8.40714069268888i	0.66	1.52	10.65	5.32	6.84	0.75	8.41	1.49E+08	71
2.00E+08	1.26E-06	0.010	4	3.54E-11	1.26E+09	-70.25	15.79	0.936225810949308+8.43352472077808i	0.94	1.07	7.48	3.74	4.81	0.75	8.43	1.49E+08	50
2.00E+08	1.26E-06	0.015	4	3.54E-11	1.26E+09	-70.25	23.69	1.39392660805306+8.4965199838243i	1.39	0.72	5.02	2.51	3.23	0.74	8.50	1.48E+08	34
2.00E+08	1.26E-06	0.025	4	3.54E-11	1.26E+09	-70.25	39.48	2.27301621714617+8.68414780910002i	2.27	0.44	3.08	1.54	1.98	0.72	8.68	1.45E+08	21
2.00E+08	1.26E-06	0.001	9	7.97E-11	1.26E+09	-158.06	1.58	6.2802455966305E-002+12.5722527875465i	0.06	15.92	111.46	55.73	71.65	0.50	12.57	1.00E+08	1115
2.00E+08	1.26E-06	0.003	9	7.97E-11	1.26E+09	-158.06	4.74	0.188388569432762+12.5735073173156i	0.19	5.31	37.16	18.58	23.89	0.50	12.57	9.99E+07	372
2.00E+08	1.26E-06	0.007	9	7.97E-11	1.26E+09	-158.06	11.05	0.439354471572043+12.5797706003403i	0.44	2.28	15.93	7.97	10.24	0.50	12.58	9.99E+07	159
2.00E+08	1.26E-06	0.010	9	7.97E-11	1.26E+09	-158.06	15.79	0.627252186054793+12.5877337638833i	0.63	1.59	11.16	5.58	7.17	0.50	12.59	9.98E+07	112
2.00E+08	1.26E-06	0.015	9	7.97E-11	1.26E+09	-158.06	23.69	0.939429552008576+12.6071457471024i	0.94	1.06	7.45	3.73	4.79	0.50	12.61	9.97E+07	75
2.00E+08	1.26E-06	0.025	9	7.97E-11	1.26E+09	-158.06	39.48	1.55815945575016+12.6682854757477i	1.56	0.64	4.49	2.25	2.89	0.50	12.67	9.92E+07	45
2.00E+08	1.26E-06	0.001	16	1.42E-10	1.26E+09	-280.99	1.58	4.71022437055501E-002+16.7628607465704i	0.05	21.23	148.61	74.31	95.54	0.37	16.76	7.50E+07	1982
2.00E+08	1.26E-06	0.003	16	1.42E-10	1.26E+09	-280.99	4.74	0.141302268821148+16.7633901141363i	0.14	7.08	49.54	24.77	31.85	0.37	16.76	7.50E+07	661
2.00E+08	1.26E-06	0.007	16	1.42E-10	1.26E+09	-280.99	11.05	0.329653268297254+16.7660356991403i	0.33	3.03	21.23	10.62	13.65	0.37	16.77	7.50E+07	283
2.00E+08	1.26E-06	0.010	16	1.42E-10	1.26E+09	-280.99	15.79	0.470838598374256+16.7694057966664i	0.47	2.12	14.87	7.43	9.56	0.37	16.77	7.49E+07	198
2.00E+08	1.26E-06	0.015	16	1.42E-10	1.26E+09	-280.99	23.69	0.705910790894713+16.7776515589117i	0.71	1.42	9.92	4.96	6.37	0.37	16.78	7.49E+07	132
2.00E+08	1.26E-06	0.025	16	1.42E-10	1.26E+09	-280.99	39.48	1.17468000391481+16.80390296625i	1.17	0.85	5.96	2.98	3.83	0.37	16.80	7.48E+07	80
4.00E+08	1.26E-06	0.001	4	3.54E-11	2.51E+09	-280.99	3.16	9.42033717601613E-002+16.7630592692026i	0.09	10.62	74.31	37.15	47.77	0.37	16.76	1.50E+08	496
4.00E+08	1.26E-06	0.003	4	3.54E-11	2.51E+09	-280.99	9.47	0.282574431703937+16.7651761129134i	0.28	3.54	24.77	12.39	15.93	0.37	16.77	1.50E+08	165
4.00E+08	1.26E-06	0.007	4	3.54E-11	2.51E+09	-280.99	22.11	0.658925132482443+16.7757403448482i	0.66	1.52	10.62	5.31	6.83	0.37	16.78	1.50E+08	71
4.00E+08	1.26E-06	0.010	4	3.54E-11	2.51E+09	-280.99	31.58	0.940569117322586+16.7891167435776i	0.94	1.06	7.44	3.72	4.78	0.37	16.79	1.50E+08	50
4.00E+08	1.26E-06	0.015	4	3.54E-11	2.51E+09	-280.99	47.37	1.4081135249842+16.8218330002052i	1.41	0.71	4.97	2.49	3.20	0.37	16.82	1.49E+08	33
4.00E+08	1.26E-06	0.025	4	3.54E-11	2.51E+09	-280.99	78.96	2.33264462805484+16.9243172018354i	2.33	0.43	3.00	1.50	1.93	0.37	16.92	1.49E+08	20
4.00E+08	1.26E-06	0.001	9	7.97E-11	2.51E+09	-632.23	3.16	6.280304364281E-002+25.1442702865738i	0.06	15.92	111.46	55.73	71.65	0.25	25.14	1.00E+08	1115
4.00E+08	1.26E-06	0.003	9	7.97E-11	2.51E+09	-632.23	9.47	0.188404429772992+25.1448976981642i	0.19	5.31	37.15	18.58	23.88	0.25	25.14	1.00E+08	372
4.00E+08	1.26E-06	0.007	9	7.97E-11	2.51E+09	-632.23	22.11	0.439555518043954+25.1480335826766i	0.44	2.28	15.93	7.96	10.24	0.25	25.15	9.99E+07	159
4.00E+08	1.26E-06	0.010	9	7.97E-11	2.51E+09	-632.23	31.58	0.627836706138562+25.1520290026781i	0.63	1.59	11.15	5.57	7.17	0.25	25.15	9.99E+07	112
4.00E+08	1.26E-06	0.015	9	7.97E-11	2.51E+09	-632.23	47.37	0.941389039783469+25.1618083083512i	0.94	1.06	7.44	3.72	4.78	0.25	25.16	9.99E+07	74
4.00E+08	1.26E-06	0.025	9	7.97E-11	2.51E+09	-632.23	78.96	1.56704070300954+25.1929752230036i	1.57	0.64	4.47	2.23	2.87	0.25	25.19	9.98E+07	45
4.00E+08	1.26E-06	0.001	16	1.42E-10	2.51E+09	-1123.97	3.16	4.71023831691392E-002+33.5256222281511i	0.05	21.23	148.61	74.31	95.54	0.19	33.53	7.50E+07	1982
4.00E+08	1.26E-06	0.003	16	1.42E-10	2.51E+09	-1123.97	9.47	0.141306033817953+33.5258869315249i	0.14	7.08	49.54	24.77	31.85	0.19	33.53	7.50E+07	661
4.00E+08	1.26E-06	0.007	16	1.42E-10	2.51E+09	-1123.97	22.11	0.329701064689074+33.5272102916759i	0.33	3.03	21.23	10.62	13.65	0.19	33.53	7.50E+07	283
4.00E+08	1.26E-06	0.010	16	1.42E-10	2.51E+09	-1123.97	31.58	0.470977823960717+33.5288971972068i	0.47	2.12	14.86	7.43	9.55	0.19	33.53	7.50E+07	198
4.00E+08	1.26E-06	0.015	16	1.42E-10	2.51E+09	-1123.97	47.37	0.706379667433154+33.5330299762005i	0.71	1.42	9.91	4.95	6.37	0.19	33.53	7.49E+07	132
4.00E+08	1.26E-06	0.025	16	1.42E-10	2.51E+09	-1123.97	78.96	1.17683591973215+33.5462377910277i	1.18	0.85	5.95	2.97	3.82	0.19	33.55	7.49E+07	79

Table 2: Using the formulas this Appendix, this Microsoft Excel spreadsheet can be used to estimate how far we can see in uniform soil using ground penetrating radar. The independent variables are in the first four columns. The spreadsheet computes the propagation constants α , β , γ , the observable depths 3.5δ (60dB) and 4.5δ (80dB), the wavelength in media λ , the velocity and the return time from a depth of 3.5δ . The spreadsheet can be downloaded from <http://www.DashFoundation.org/HowDeep/MaxDepth.zip>.

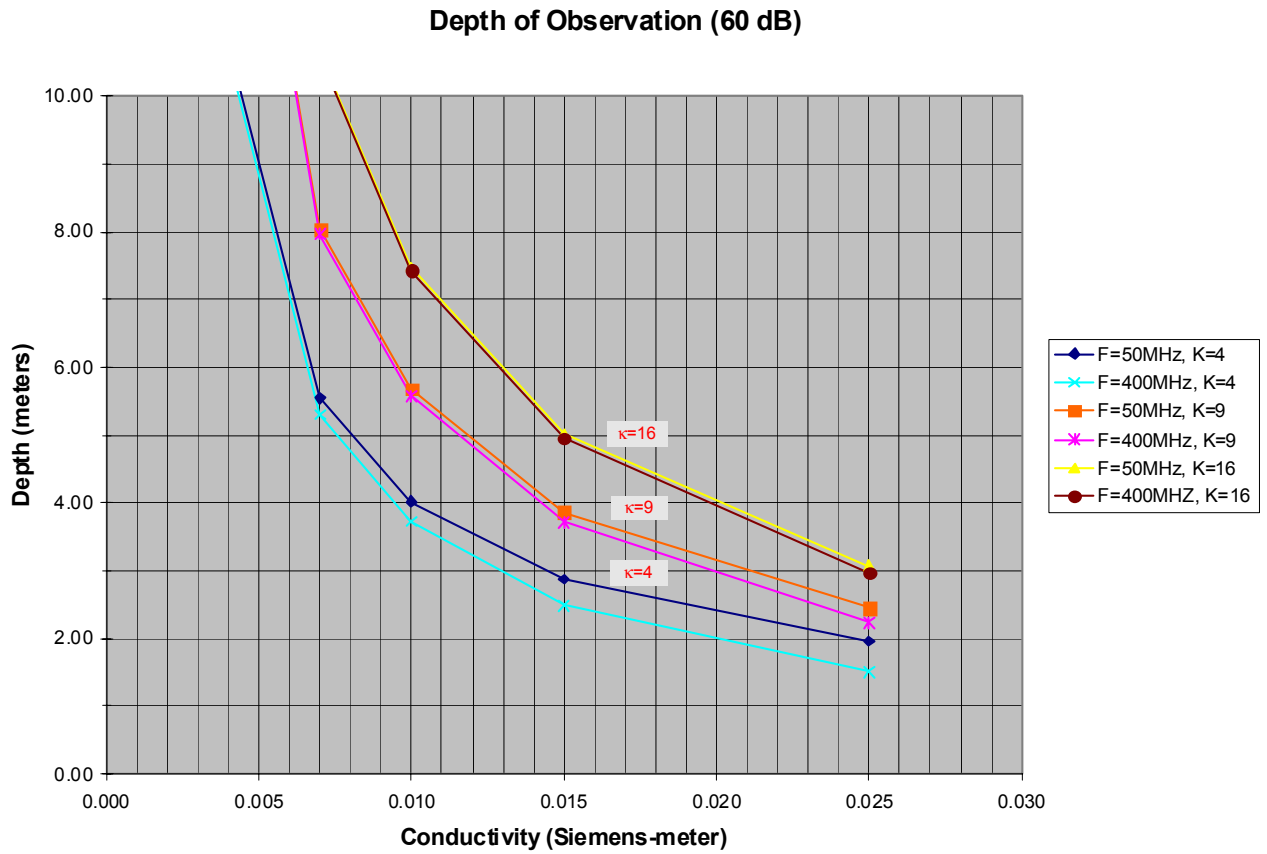


Figure 22: These six curves show the theoretical maximum depth of observation for several uniform soil types ($\mu=\mu_0$) where the maximum loss which can be tolerated is 60 dB. The depth of observation is a function of conductivity and permeability, but only in relatively conductive soils does the transmitting frequency much matter.

Or, if our preference is to use milli-Siemens:

$$\frac{19\sqrt{\kappa}}{\sigma_m} > Depth > \frac{24\sqrt{\kappa}}{\sigma_m}$$

Where:

σ_m = Conductivity in milli-Siemens

Soils of this type are known as *dielectric* or *non-dispersive* soils. They are the soils for which archaeological geophysics proves the most productive.

To predict the radar's performance at a particular site where the characteristics of the strata are known, we need to calculate the loss due to each stratum the signal passes through. We can use this formula:

$$E = E_0 e^{-\alpha x}$$

$$Loss = \frac{E}{E_0} = e^{-\alpha x}$$

$$Loss(dB) = -20 \log(e^{-\alpha x}) = 8.7 \alpha x$$

Where the soil is of the dielectric type:

$$Loss(dB) = 8.7 \left[\frac{188.5\sigma}{\sqrt{\kappa}} \right] x = \frac{1637\sigma}{\sqrt{\kappa}} x$$

Or, in milli-Siemens:

$$Loss(dB) = \frac{1.64\sigma_m}{\sqrt{\kappa}} x$$

Or in terms of decibels per meter:

$$\boxed{Loss(db/m) = \frac{1.64\sigma_m}{\sqrt{\kappa}}}$$

We can simplify the formula for velocity as well: The velocity is:

$$v = \frac{\omega}{\beta} = \frac{\omega}{\text{Im} \sqrt{j\omega\mu\sigma - \omega^2\mu\epsilon}}$$

Again, where $\sigma \ll \omega\epsilon$ and $\mu = \mu_0$:

$$|j\omega\mu\sigma| \ll |\omega^2\mu\epsilon|$$

$$v = \frac{\omega}{\text{Im}\sqrt{-\omega^2\mu\epsilon}} = \frac{1}{\sqrt{\mu\epsilon}} = \frac{1}{\sqrt{\mu_0\epsilon_0}\sqrt{\kappa}}$$

But note that:

$$\frac{1}{\sqrt{\mu_0\epsilon_0}} = \frac{1}{\sqrt{(4\pi \times 10^{-7})(8.85 \times 10^{-12})}} = 3 \times 10^8 \text{ m/sec}$$

This is the speed of light. That makes sense since a wave traveling in a vacuum ($\epsilon=\epsilon_0$, $\mu=\mu_0$) should be traveling at the speed of light. Therefore, in the dielectric case the velocity can be more simply stated to be:

$$v = \frac{c}{\sqrt{\kappa}}$$

Where:

$$c = \text{speed of light} = 3 \times 10^8 \text{ m/s}$$

In the case where $\sigma \gg \omega\epsilon$, we are dealing with *conductive*, as opposed to dielectric, soils, also known as *dispersive* soils. This situation is quite different. In conductive soils (Krause 1992: 550):

$$\alpha = \text{Re}\sqrt{j\omega\mu\sigma - \omega^2\mu\epsilon}$$

$$\sigma \gg \omega\epsilon$$

$$\alpha = \text{Re}\sqrt{j\omega\mu\sigma}$$

$$\sqrt{j} = \sqrt{\frac{2j}{j}} = \sqrt{\frac{1+2j-1}{2}} = \frac{1+j}{\sqrt{2}}$$

$$\alpha = \sqrt{\frac{\omega\mu\sigma}{2}}$$

$$\delta = \frac{1}{\alpha} = \sqrt{\frac{2}{\omega\mu\sigma}} = \frac{1}{\sqrt{f\pi\mu\sigma}}$$

In this case, delta (δ) is referred to as the *skin depth*. In conductive media, electromagnetic waves tend to be confined to the near surface, forming a skin of current. Most importantly, unlike the dielectric case, the skin depth is a function of frequency. The higher the frequency of the signal, the less penetration we can achieve.

As for the velocity in the conductive case:

$$\sigma \gg \omega\epsilon$$

$$v = \frac{\omega}{\text{Im}\sqrt{j\omega\mu\sigma}}$$

But :

$$\sqrt{j} = \frac{1+j}{\sqrt{2}}$$

So :

$$v = \frac{\sqrt{2}}{\text{Im}(1+j)} \frac{\omega}{\sqrt{\omega\mu\sigma}} = \sqrt{\frac{2\omega}{\mu\sigma}}$$

Note the important distinction here. In the dielectric case, all radio frequency energy, regardless of its frequency, travels at the same speed. In the conductive case, different frequency components travel at different speeds, resulting in a returning radar signal which is smeared, or dispersed. In dispersive soils, impulse radars work poorly. Signals become smeared and resolution lost.

Appendix B: Loss in Translation

We use Greek letters to denote electrical parameters such as conductivity (σ) and permittivity (ϵ). But unless we use these terms precisely, their meaning can be lost in translation. In order to avoid confusion, we need to remember exactly what is meant by conductivity and permittivity.

Conductivity is a measure of how easily electrons travel through a medium. Electrons are negatively charged, and are propelled by electric fields. Their movement results in an electric current, whose density we denote by the letter J :

$$J = \sigma E$$

Where:

J = Current density in Amperes per square meter

σ = Conductivity in Siemens per meter (= mhos/meter)

E = Electric field in Volts per meter

Consider a volume of material one meter in length, width and height (Figure 23). We can restate the above relationship through its circuit equivalent, Ohm's law, by (1) multiplying the current density by the conductor's area A , thereby deriving the current I , (2) multiplying electric field by the conductor's length d , thereby deriving the voltage V , and dividing the two to derive the conductance G :⁷

$$I = J \cdot A$$

$$V = E \cdot d$$

However :

$$A = d = 1$$

Therefore :

$$G = \sigma$$

$$I = VG$$

⁷ The formula for the conductance of a volume of material is:

$$G = \frac{A\sigma}{d}$$

Where:

A = Area of the conductor in square meters

d = Length of the conductor in meters

Where $A=d=1$, $G=\sigma$.

Similarly, the formula for the capacitance of a parallel plate capacitor is:

$$C = \frac{A\epsilon}{d}$$

In our example, $A=1$ and $d=1$, so $C=\epsilon$

Permittivity is a measure of how easily a medium can be electrically charged. We can charge a medium by applying an electric field and measuring how much charge accumulates.

$$\epsilon E = \rho$$

Where:

E = Electric field in Volts per meter

ϵ = Permittivity in Farads per meter

ρ = Charge density in Colombes per square meter

Again, we can state this formula in its circuit equivalent by multiplying by the appropriate dimensions:

$$CV = Q$$

Where:

C = Capacitance in Farads

V = Volts

Q = Charge in Colombes

We can measure the conductivity and the permittivity of a block of soil using the apparatus in Figure 23. Here one cubic meter of soil is placed between two plates and a voltage applied. After the current stabilizes we can derive the conductivity.

$$I = VG$$

$$\sigma = G = \frac{I}{V}$$

Next, we can disconnect the source and measure the time it takes for the voltage to decay to 36.8% of its initial value. This period of time is known as the “time constant” and is equal to ϵ/σ . That yields the permittivity.

$$\tau = \frac{\epsilon}{\sigma}$$

$$\epsilon = \sigma\tau$$

Where:

τ = Time Constant (time for voltage to fall to 36.8% of initial value)

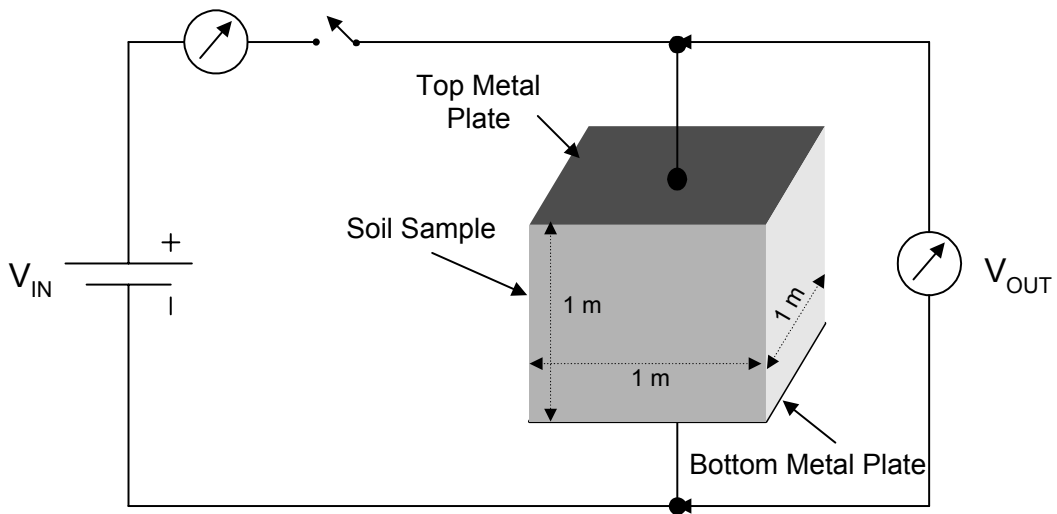
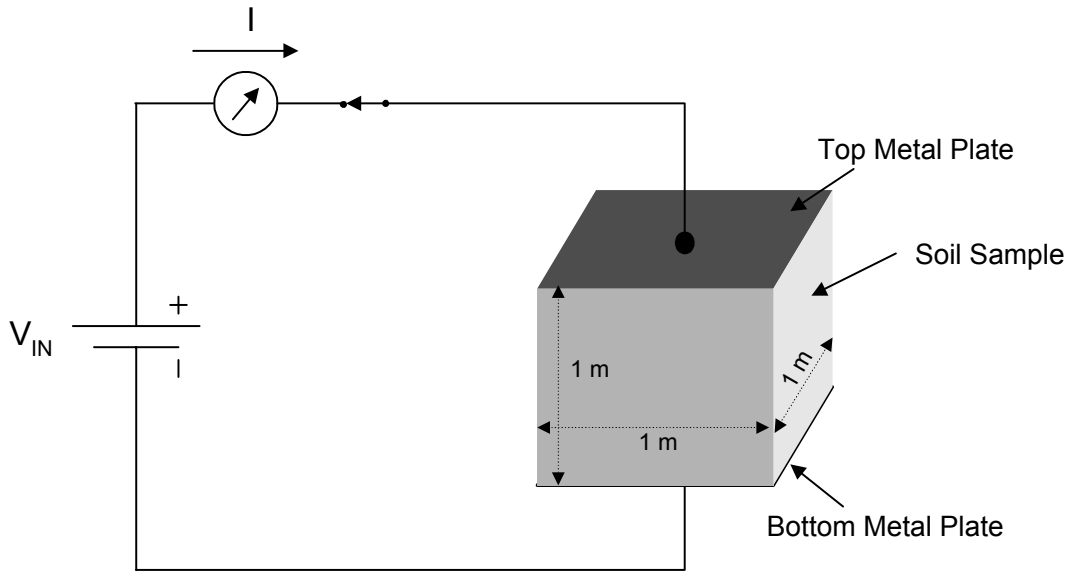


Figure 23: Conductivity (σ) and permittivity (ϵ) can be measured using this apparatus. At the top, a voltage is applied to one cubic meter of soil and the current measured. The ratio of current to voltage is equal to the conductivity. At the bottom, the cube, having previously been charged to voltage V_{IN} is allowed to discharge. The time it takes for the voltage V_{OUT} to fall to 36.8% of its initial value is the time constant τ . The permittivity ϵ can be calculated from the formula $\epsilon = \sigma\tau$.

Current that flows as a result of the volume's conductivity is dissipated in the form of heat. Current that flows as a result of the volume's permittivity is stored and not dissipated. This energy storage capacity (or *capacitance*) is due to the complex nature of matter. Most matter is made up of polar molecules which turn to oppose the polarity of the applied field. In doing so, these molecules are also stretched slightly. Just as stretched springs store energy, so do the molecules.

When we move from direct current (static analysis) to alternating currents (dynamic analysis) the situation gets more complex (Figure 24). In circuit terms, our sample has a capacitance equal to ϵ and a conductance equal to σ . If we sweep the frequency of our source, we will find that the current through our sample varies with frequency as follows:

$$I = V_{IN}(j\omega\epsilon + \sigma)$$

As shown in Figure 24, the equivalent circuit is a capacitor of value ϵ in parallel with a resistor of conductance σ . At low frequencies, we are in the dissipative region and most of the current flows through the resistor. At high frequencies, we enter the dielectric region and most of the current flows through the capacitor.

As stated, it is the conductivity of the soil that causes dissipation. The current that flows through the capacitance is not dissipated, but temporarily stored. However, as noted, when alternating currents are applied to a sample, the polar molecules that make up the capacitance swing back and forth as the applied polarity changes. Along with providing the means for energy storage, that movement causes friction among the molecules and that friction causes heating. The higher the frequency of the signal, the faster the molecules move and the greater the heating.

To include this "dielectric heating" in our model, we add another dissipative element to our formula. The current in our model becomes:

$$I = V_{IN}(j\omega\epsilon + \sigma_c + \sigma_d)$$

Where:

σ_c = Conductance causing conduction heating

σ_d = Conductance causing dielectric heating

Experimentally, dielectric heating is a function of the permittivity and the frequency. We can model it by dividing the permittivity into two parts, ϵ' and ϵ'' , one real and one imaginary. The real part (ϵ') represents the capacitive element, the imaginary part (ϵ'') the dissipative:

$$\begin{aligned} \text{Let :} \\ \epsilon &= \epsilon' - j\epsilon'' \\ j\omega\epsilon &= j\omega\epsilon' + \omega\epsilon'' \\ I &= V_{IN}(j\omega\epsilon' + \sigma_c + \omega\epsilon'') \\ \sigma_d &= \omega\epsilon'' \end{aligned}$$

As a practical matter, it is very difficult to measure losses due to dielectric heating separate and apart from those due to conduction. When we measure, we end up with a combination of the two, an *apparent* conductivity:

$$\sigma_{app} = \sigma_c + \omega\epsilon''$$

Therefore:

$$I = V_{IN}(j\omega\epsilon' + \sigma_{app})$$

Returning to our circuit model, we can now remodel our soil sample as a combination of a capacitor $C=\epsilon'$ in parallel with a conductance of σ_{app} . This is, in fact, what we measure when we test a soil sample. We observe a current that increases with frequency, rising more steeply at frequencies above $\omega=\sigma_{app}/\epsilon'$.

The confusion we referred to above arises from a commonly used re-definition. We can remove σ from the equation entirely by re-defining the imaginary part of the permittivity, ϵ'' , to include conductivity, σ_c . We create a new product of variables, $\omega\epsilon''_{app}$, equal to:

$$\omega\epsilon''_{app} = \sigma_{app}$$

Using this re-definition, our current becomes:

$$\begin{aligned} I &= V_{IN}(j\omega\epsilon' + \omega\epsilon''_{app}) \\ I &= j\omega V_{IN}(\epsilon' - j\epsilon''_{app}) \end{aligned}$$

The magnitude of our current is:

$$|I| = \omega V_{IN} \sqrt{(\epsilon')^2 + (\epsilon''_{app})^2}$$

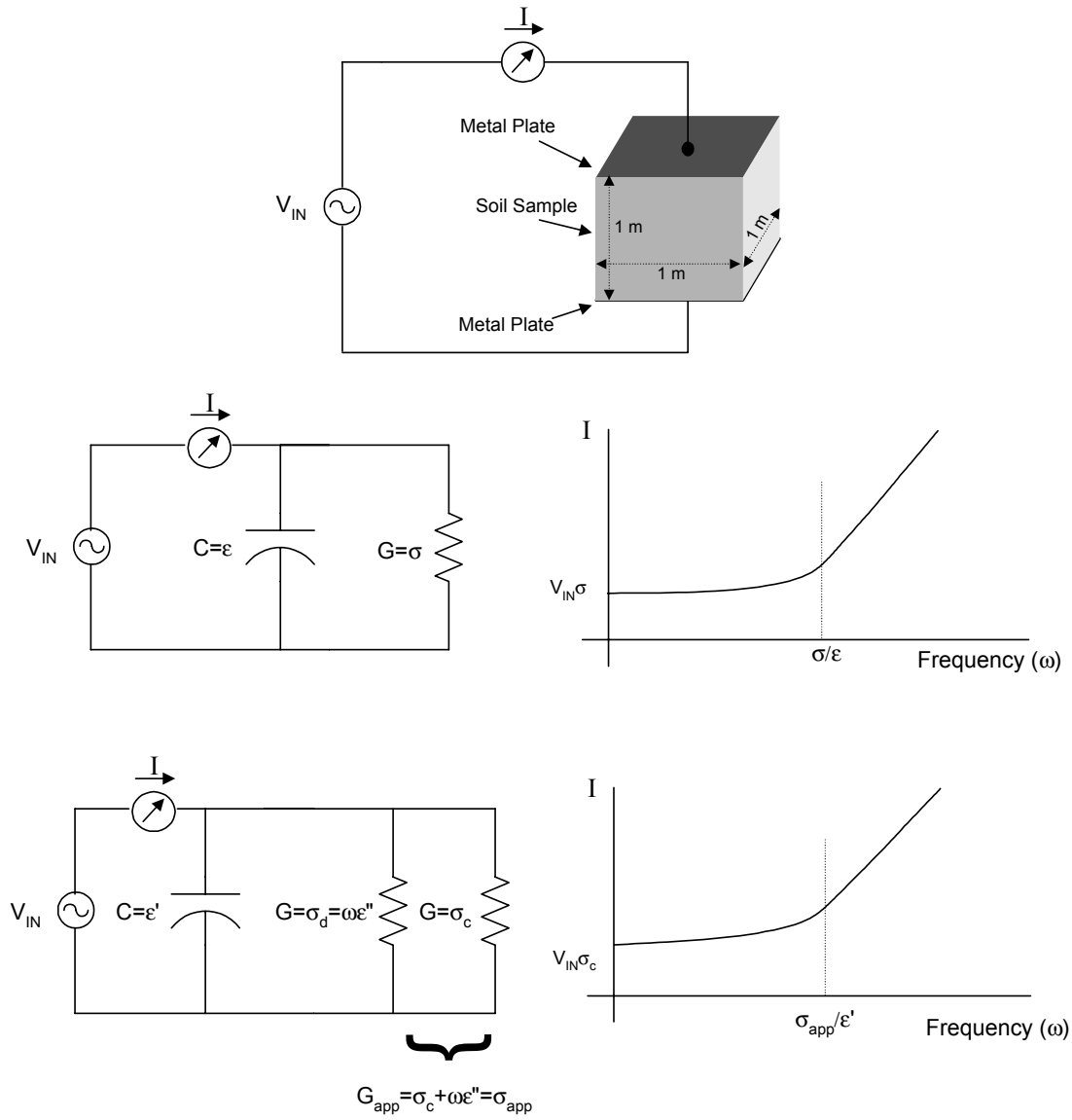


Figure 24: Conduction and dielectric currents. In a simplified model, current is dominated by conductivity (σ) at low frequencies and permittivity (ϵ) at higher frequencies. A more complete model includes dielectric losses.

The phase of the current relative to the voltage is (Figure 25):

$$\delta = \tan^{-1} \left(\frac{\epsilon''_{app}}{\epsilon'} \right)$$

Published tables of the material properties of soils and other media typically have only two entries, ϵ' and the *loss tangent*. From these we derive the conductivity and the permittivity. The loss tangent is defined as:

$$\tan \delta = \frac{\epsilon''_{app}}{\epsilon'}$$

However, it is important to remember that the loss tangent is a function of ϵ''_{app} , which is, in turn, a function of both conduction and dielectric losses.

Note also that if we define a new variable, ϵ_{app} to be equal to:

$$\epsilon_{app} = \epsilon' - j\epsilon''_{app}$$

Then:

$$\sigma_{app} = \text{Re}(j\omega\epsilon_{app})$$

One often sees this equation in the published literature. However, it is important to remember that this equation includes conductivity within the definition of apparent permittivity. If we do not include conductivity within the definition of apparent permittivity, then conductivity and permittivity remain separate and independent variables.

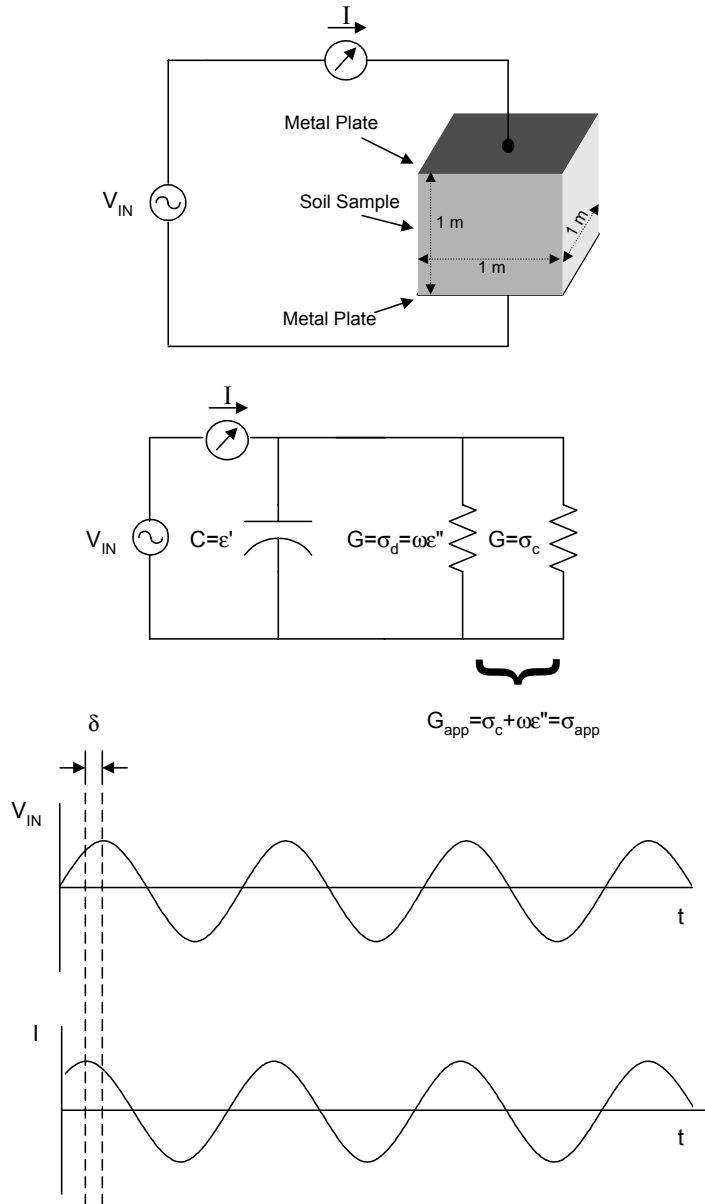
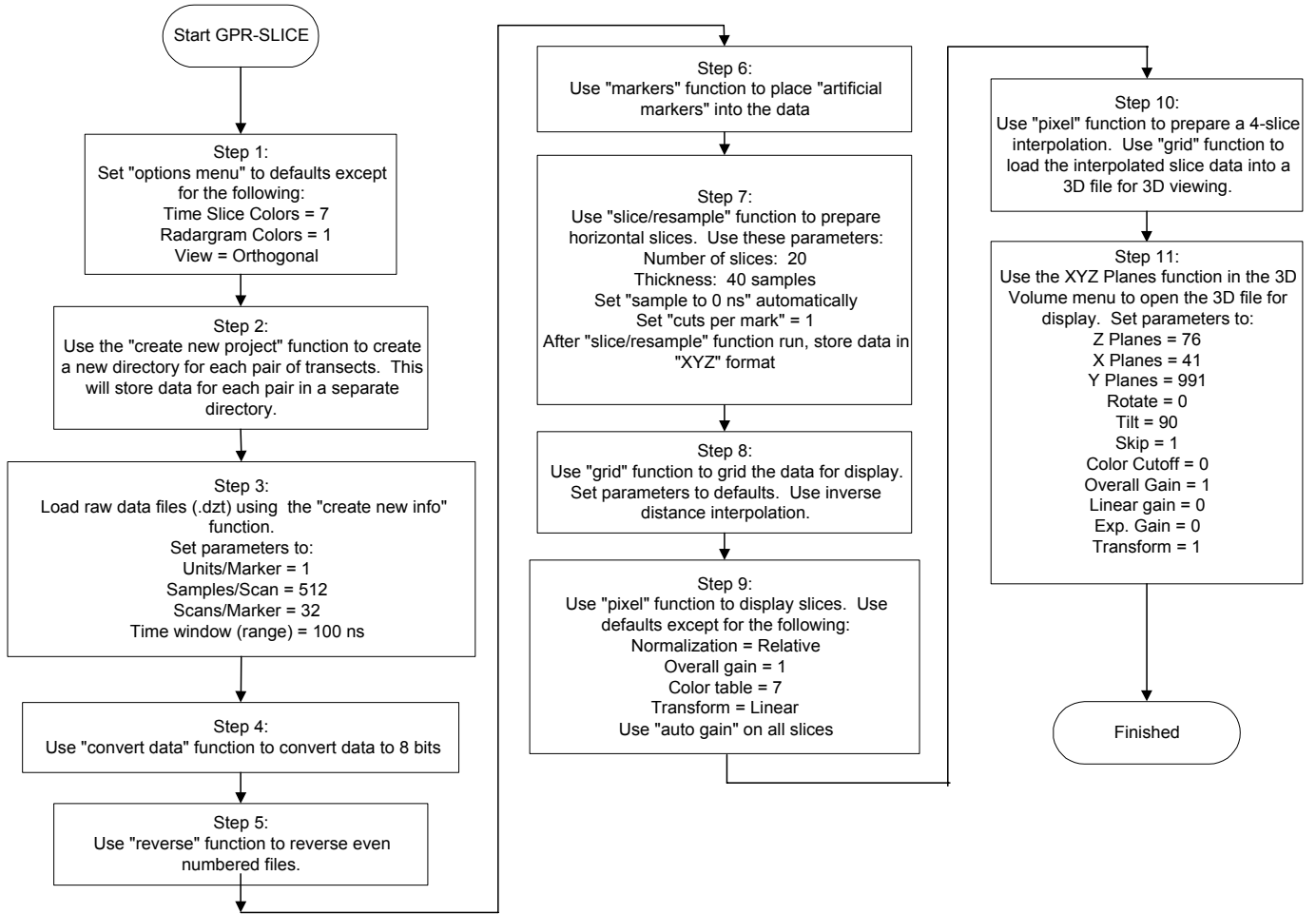


Figure 25: Conductivity, permittivity and phase. The phase delay δ and the ratio of the current I to the voltage V_{IN} are used to derive the material's apparent conductivity and permittivity.

Appendix C: GprMax2D Input File

```
#medium: 4.0 0.0 0.0 0.005 1.0 0.0 stratum_2
#medium: 5.7 0.0 0.0 0.007 1.0 0.0 stratum_3
#medium: 7.5 0.0 0.0 0.009 1.0 0.0 stratum_4
#medium: 10.0 0.0 0.0 0.012 1.0 0.0 stratum_5
-----
#domain: 10.0 10.0
#dx_dy: 0.01 0.01
#time_window: 150.0e-9
-----
#box: 0.0 0.0 10.0 3.2 stratum_5
#box: 0.0 3.2 10.0 3.6 stratum_4
#box: 0.0 3.6 10.0 5.8 stratum_3
#box: 0.0 5.8 10.0 8.0 stratum_2
#box: 0.0 8.0 10.0 10.0 free_space
#box: 3.0 0.7 7.0 2.7 free_space
-----
#line_source: 1.0 200e6 ricker MySource
#analysis: 1 MGOutput.out a
#tx: 4.8 8.0 MySource 0.0 150e-9
#rx: 5.2 8.0
#end_analysis:
#title: Full Wave Simulation at Mersa/Wadi Gawasis
#messages: y
```

Appendix D: Flowchart for Processing Data in GPR Slice



References

- Bard, K. A. and Fattovich, R.
2007. *Harbor of the Pharaohs to the Land of Punt*. Naples: Universita Degli Studi di Napoli "L'Orientale."
- Breasted, J. H.
1906-7. *Ancient Records of Egypt, I-V*. Reprint 1962. New York: Russel & Russel.
- Bradbury, L.
1988. "Reflections on Traveling to 'God's Land' and Punt in the Middle Kingdom," *JARCE* 25:127-156.
- Clayton, P.
1994. *Chronicles of the Pharaohs*. London: Thames and Hudson.
- Daniels, D.
2004. *Ground Penetrating Radar, Second Edition*. London: IEE.
- Dash, G.
2005-2006. Field Notes.
- Jones, D.
1995. *Boats*. Austin: University of Texas Press.
- Kraus, J.
1992. *Electromagnetics, Fourth Edition*. New York: McGraw-Hill.
- Naville, E.
1898. *The Temple of Deir el Bahari III*. London: Egypt Exploration Society.
- Sayed, A. M.
1977. "Discovery of the Site of the 12th Dynasty Port at Wadi Gawasis on the Red Sea Shore," *RE* 29: 140-178.
- Sayed, A. M.
1978. *The Discovery of the Twelfth Dynasty Port in the Region of the Wadi Gawasis on the Red Sea Coast* (in Arabic). Alexandria: University of Alexandria.
- Sayed, A. M.
1979a. "Discovery of the Site of the 12th Dynasty Port at Wadi Gawasis on the Red Sea Shore." W. F. Reineke (ed.), *Acts of the First International Conference of Egyptology*. Berlin: Akademie Verlag, pp. 569-578.

- Sayed, A. M.
1979b. "New Light on the Recently Discovered Port on the Red Sea Shore."
Second International Conference of Egyptology. Grenoble, abstract.
- Sayed, A. M.
1980. "Observations on Recent Discoveries at Wadi Gawasis," *JEA* 66: 154-157.
- Sayed, A. M.
1983. "New Light on the Recently Discovered Port on the Red Sea Shore,"
Chronique d'Egypte 58: 23-37.
- Sayed, A. M.
1999. "Wadi Gawasis." K. A. Bard (ed.), *Encyclopedia of the Archaeology of Ancient Egypt*. London: Routledge, pp. 866-868.
- Sayed, A. M.
2003. "The Land of Punt: Problems of the Archaeology of the Red Sea and Southern Delta." Zahi Hawass (ed.), *Egyptology at the Dawn of the Twenty First Century*. Cairo: The American University in Cairo Press, pp. 432-439.
- Tregenza, L. A.
1958. *Egyptian Years*. London: Oxford University Press.
- Vining, Benjamin
2005-2006. Field Notes.
- Vining, Benjamin
2006-2007. Field Notes.
- Vinson, S.
1994. *Egyptian Boats and Ships*. Buckinghamshire: Shire Publications.
- Ward, C.
2000. *Sacred and Secular, Ancient Egyptian Ships and Boats*. Boston: Archaeological Institute of America.